Investigation of the global translational response to oxidative stress in the model archaeon *Haloferax volcanii* reveals untranslated small RNAs with ribosome occupancy

Emma Dallon[a], Haley M. Moran[b], Sadhana R. Chidambaran[a], Arman Kian[a], Betty Y.H. Huang[a], Stephen D. Fried[b,c], Jocelyne DiRuggiero[a,d*]

[a] Department of Biology, Johns Hopkins University, Baltimore, Maryland, USA

[b] Department of Chemistry, Johns Hopkins University, Baltimore, Maryland, USA

[c] T. C. Jenkins Department of Biophysics, Johns Hopkins University, Baltimore, Maryland, USA

[d] Department of Earth and Planetary Sciences, Johns Hopkins University, Baltimore, Maryland, USA

*Corresponding author: Jocelyne DiRuggiero

Email: jdiruggiero@jhu.edu

Abstract

Oxidative stress induces a wide range of cellular damage, often causing disease and cell death. While many organisms are susceptible to the effects of oxidative stress, haloarchaea have adapted to be highly resistant. Several aspects of the haloarchaeal oxidative stress response have been characterized, however little is known about the impacts of oxidative stress at the translation level. Using the model archaeon *Haloferax volcanii*, we performed RNA-seq and ribosome profiling (Ribo-seq) to characterize the global translation landscape during oxidative stress. We identified 281 genes with differential translation efficiency (TE). Downregulated genes were enriched in ribosomal and translation proteins, in addition to peroxidases and genes involved in the TCA cycle. We also identified 42 small noncoding RNAs (sRNAs) with ribosome occupancy. Size distributions of ribosome footprints revealed distinct patterns for coding and noncoding genes, with 12 sRNAs matching the pattern of coding genes, and mass spectrometry confirming the presence of seven small proteins encoded in these sRNAs. However, the majority of sRNAs with ribosome occupancy had no evidence of coding potential. Of these ribosome-associated sRNAs, 12 had differential ribosome occupancy or TE during oxidative stress, suggesting that they may play a regulatory role during the oxidative stress response. Our findings on ribosomal regulation during oxidative stress, coupled with potential roles for ribosome-associated noncoding sRNAs and sRNA-derived small proteins in *H. volcanii*, revealed additional regulatory layers and underscore the multifaceted architecture of stress-responsive regulatory networks.

Importance: Archaea are found in diverse environments, including as members of the human microbiome, and are known to play essential ecological roles in major geochemical cycles. The study of archaeal biology has expanded our understanding of the evolution of eukaryotes, uncovered novel biological systems, and revealed new opportunities for applications in biotechnology and bioremediation. Many archaeal systems, however, remain poorly characterized. Using *Haloferax volcanii* as a model, we investigated the global translation landscape during oxidative stress. Our findings expand current knowledge of translational regulation in archaea and further illustrate the complexity of stress-responsive gene regulation.

Introduction

Since the advent of oxygenic metabolism, oxidative stress has affected most organisms across all domains of life. This stress is associated with reactive oxygen species (ROS) that disrupt cellular redox state and covalently damage essential macromolecules (1-3). While endogenous ROS, including hydrogen peroxide and superoxide, arise as byproducts of oxygen metabolism (1), ROS levels can increase due to environmental stressors (1, 4). Prolonged oxidative stress induces a range of responses, including disease, autophagy, and cell death (5-8). To neutralize ROS, prokaryotes utilize numerous enzymes (9-13), and certain bacteria and archaea, such as haloarchaea, are known to be exceptionally resistant to oxidative stress (4, 14-17).

Archaea have attracted interest because of mounting evidence that they are ancestral to eukaryotes (18). This is reflected in the mosaic nature of archaeal cells with prokaryotic features and yet information processing machinery more closely related to that of eukaryotes (18-20). The study of archaea has led to the discovery of novel biological systems, such as unique lipids and protein modifications not found in other domains (21, 22). These findings shed light on the evolution of eukaryotes from a prokaryotic ancestor (23) and expand possibilities for biotechnology applications (24). However, many archaeal regulatory systems remain poorly characterized, and our knowledge of them lags behind that of bacterial and eukaryotic counterparts. For example, mechanisms of transcriptional regulation, especially in response to oxidative stress, have only been studied in a few archaeal species (25-27). In the model archaeon, *Haloferax volcanii*, a key transcriptional regulator, RosR, was shown to affect the expression of many genes in response to oxidative stress (26). However, while RosR is conserved among haloarchaea, its function varies among species (25). Gene regulation at the post-transcriptional level by small noncoding RNAs (sRNAs) is particularly critical to stress responses in many prokaryotic organisms (28-31), and has been linked to oxidative stress in several bacteria (32-34) and in the archaeon *H. volcanii* (27, 35). In *H. volcanii*, the most upregulated sRNA during oxidative stress (SHOxi) binds and destabilizes malic enzyme transcripts, leading to higher cell survival rates during oxidative stress (35).

While many studies have characterized mechanisms of oxidative stress response at the transcriptional, post-transcriptional, and post-translational levels, little is known about the impacts of oxidative stress at the translation level. Translational regulation has been shown to play a major role in various stress conditions in both bacteria and yeast (36-39). In yeast, the global translation landscape during oxidative stress has been explored using ribosome profiling (Ribo-seq), revealing the regulation of several individual genes and general shifts in translation patterns across all genes (40). Mechanisms of translational regulation by proteins and sRNAs during stress have also been reported in archaea. The archaeal protein IF6, a homolog to eukaryotic IF6, inhibits translation by binding to the large ribosomal subunit, preventing assembly of the full ribosome, and is overexpressed during thermal stress (41). In *Methanosarcina mazei*, sRNAs were shown to mask the ribosome binding site of target mRNAs to modulate translation in response to nitrogen starvation (42, 43). This mechanism bears resemblance to an oxidative stress-responsive sRNA in *E. coli* (44). Additionally, proteomic studies in *H. volcanii* have begun to elucidate the differences between transcription and

translation during stress responses (45, 46). However a comprehensive study of translational regulation during oxidative stress response has thus far been lacking.

In this work we present evidence of translational regulation during oxidative stress in *H. volcanii*. This model archaeon is well-characterized at the genetic level (47-49) and a variety of genetic and biochemical tools are available for its manipulation (50, 51). Recent advances in translation research in *H. volcanii* (52, 53) have demonstrated that Ribo-seq enables the detection of translational changes, providing a means to probe the impact of oxidative stress on protein synthesis. In the present work, we combined RNA sequencing (RNA-seq) and ribosome profiling (Ribo-seq) to determine the global translation landscape during oxidative stress response. We identified genes that are differentially regulated at the translation level under oxidative stress and, using an integrative approach, investigated the potential role of stress-responsive ribosome-associated sRNAs and sRNA-encoded small proteins.

Results

We investigated the global translation landscape in *H. volcanii* during oxidative stress by performing RNA-seq and Ribo-seq *on H. volcanii* cultures with and without stress treatment. Ribo-seq, a technique that captures ribosome occupancy across thousands of transcripts, can be used as a proxy for translation (54). By comparing transcription levels from RNA-seq data to ribosome occupancy from Ribo-seq data, we assessed differential expression, ribosome occupancy, and translation efficiency, allowing us to identify genes regulated at the translation level. Using this integrated approach, we also identified ribosome-associated sRNAs responsive to oxidative stress.

Hundreds of genes, including known oxidative stress-responsive genes, had differential ribosome occupancy during oxidative stress.

Libraries for RNA-seq and Ribo-seq were prepared from four biological replicate cultures treated with 2 mM hydrogen peroxide for one hour to induce oxidative stress, as previously described (27, 35). Four replicates without stress treatment were used as controls. Sequenced reads were aligned to the genome (49) and normalized expression values of transcripts per million (TPM) were calculated (Table S1, Table S2). Using a minimum detection cutoff of 10 TPM per gene, averaged across all biological replicates, we detected 84% of annotated genes in both RNA-seq control and stress samples. For the Ribo-seq data, we detected 74% of annotated genes in control samples and 80% in stress samples.

We calculated differential expression between controls and oxidative stress treatments for the RNA-seq and Ribo-seq datasets (Table S3). Genes with an adjusted p-value <0.05 and an absolute $\log_2$ fold change >1 were considered differentially expressed during oxidative stress. Lowly expressed genes with TPM <10 in both conditions were excluded from the analysis. We found 559 genes with differential RNA expression during oxidative stress, in contrast to 966 genes with differential ribosome occupancy (Fig. 1A, B).

131 To validate our experimental approach, we investigated the differential expression of five
132 previously known oxidative stress-responsive genes. These genes were for superoxide
133 dismutase (HVO_RS03960), catalase (HVO_RS13250), a universal stress protein
134 (HVO_RS06755), and a ssDNA binding replication protein (HVO_RS06110); the latter two were
135 both reported as upregulated proteins in *H. volcanii* under hypochlorite stress (46). All showed
136 significant upregulation in both RNA-seq and Ribo-seq datasets (Fig1A, B; Table S4), implying
137 our experimental approach recapitulated known aspects of oxidative stress response. We also
138 observed upregulation of a gene involved in metal homeostasis (HVO_RS07285; Fig1A, B; Table
139 S4) and downregulation of four others (HVO_RS00195-210; HVO_RS07290; Fig1A, B; Table S4),
140 consistent with previous findings (46).
141
142 We then tested the hypothesis that genes with differential transcript expression would have
143 differential ribosome occupancy, as transcripts highly abundant during oxidative stress would
144 likely be bound by a higher number of ribosomes than transcripts with low abundance. By
145 comparing significant gene lists from RNA-seq and Ribo-seq data, we identified 320 genes with
146 both differential RNA expression and ribosome occupancy during stress. The remaining 646
147 genes changed only in ribosome occupancy during stress (67% of all genes with differential
148 ribosome occupancy; Fig. S1). Several genes had differential ribosome occupancy in accordance
149 with previously published proteomics data [HVO_RS02870-*msrA;* HVO_RS04695-cysteine
150 desulfurase; Table S3; (46)]. Overall, in both RNA-seq and Ribo-seq datasets, we detected the
151 majority of annotated genes and identified hundreds of genes with differential ribosome
152 occupancy during oxidative stress.
153
154 **Translation efficiency revealed global downregulation of translation during oxidative stress.**
155 To increase the stringency of our analysis and identify genes that were regulated uniquely at
156 the translation level, we calculated translation efficiency (TE). This quantity is defined as the
157 ratio between the Ribo-seq fold change and the RNA-seq fold change and was used for
158 differential expression analysis (Table S3). TE values account for changes in transcript
159 availability and identify genes that change at the Ribo-seq and/or RNA-seq level while
160 eliminating those that change proportionally in both. We found 281 genes with significant
161 differential TE (Fig. 1C; adjusted p-value <0.05, absolute $\log_2$ fold change >1). When comparing
162 genes with differential TE to those with differential transcript expression and differential
163 ribosome occupancy, we found that 240 genes (85.4%) were regulated only at the level of
164 translation (Fig. S2). The remaining 41 genes were regulated at both the transcriptional and
165 translational levels, with 30 genes displaying opposing effects at each level (Table S3). The
166 majority (66.7%) of genes with opposing effects were upregulated at the transcriptional level
167 yet downregulated at the translational level. Of the 281 genes with differential TE, 29.9% were
168 upregulated and 70.1% were downregulated during oxidative stress (Table S5).
169
170 We investigated some basic properties of transcripts with differential TE to determine whether
171 they were distinct from the overall transcriptome. We found no differences in amino acid or
172 codon frequencies (Fig. S3) and no difference in the proportion of leaderless transcripts
173 compared to the whole transcriptome (Table S5), most likely because *H. volcanii* translation
174 initiation is not dependent on the presence of a 5'UTR (55). The average size for genes with

differential TE was slightly smaller, likely due to a narrower size range of significant genes (Table S5).

We next investigated whether genes with differential TE during oxidative stress exhibited functional enrichments. Gene ontology (GO) analysis was performed using PANTHER generic mapping (56, 57), with enrichment significance determined via Fisher's test and false discovery rate (FDR correction). Additionally, KEGG pathway enrichment analysis was conducted using the STRING database (58). Both PANTHER and STRING rely on homology-based functional predictions. Approximately half of all annotated *H. volcanii* genes were assigned to functional categories using PANTHER (Table S6). However, few significant functional enrichments were observed among genes with differential TE, likely due to small sample size (Fig. 1D, Table S7). Among genes with downregulated TE during oxidative stress, we observed significant enrichment of translation-related functions (Fig. 1D). Specifically, GO enrichment analysis revealed overrepresentation of ribosomal proteins (fold enrichment = 4.41, FDR = 0.0005) and translation-associated proteins (fold enrichment = 3.39, FDR = 0.0008). Consistent with these results, KEGG pathway analysis also identified significant enrichment of ribosomal proteins (FDR = 0.00093). In addition, we observed differential TE for many genes associated with redox homeostasis. Notably, downregulated genes showed enrichment of peroxidases (GO; fold enrichment = 9.5, FDR = 0.0213) and tricarboxylic acid (TCA) cycle components (KEGG; FDR = 0.0242). In contrast, no statistically significant functional enrichment was detected among genes with upregulated TE during oxidative stress (Fig. 1D).

In addition to analyzing functional categories of genes with differential TE, we sought to identify whether specific cellular pathways were subject to translational regulation during oxidative stress. To do so, we used the STRING database to predict interaction networks for genes with upregulated or downregulated TE. Few predicted interactions were identified among upregulated genes (Fig. S4A). In contrast, genes with downregulated TE formed a larger, interconnected network with many functional clusters (Fig. S4B). The two largest clusters were composed of ribosome-associated genes, including numerous ribosomal proteins, and genes involved in the TCA cycle. Additional smaller clusters, with four genes each, were related to oxidative phosphorylation, pyrimidine biosynthesis, and putative translation initiation factors. These interaction networks suggest that while global translation is broadly reduced under oxidative stress, specific pathways are subject to targeted translational regulation, likely to modulate metabolic activity and maintain cellular homeostasis.

While the majority of genes with differential TE were regulated only at the translational level, 15% of genes with differential TE exhibited changes (absolute $\log_2$ fold change >1) at both the transcriptional and translational levels. One such gene, HVO_RS04895, encoding a protein with a transmembrane domain, showed increased ribosome occupancy and TE (Table S8). This gene is known to be transcriptionally upregulated during oxidative stress via the transcriptional regulator OxsR (59). We also identified two genes with a distinct regulation pattern characterized by downregulated TE, coupled with increased RNA expression and ribosome occupancy (Table S8). These genes encode KatG (HVO_RS13250), a catalase/peroxidase that uses hydrogen peroxide as its substrate (60, 61), and DpsA (HVO_RS07285), a DNA

219 starvation/stationary phase protection protein (62, 63). Previous proteomics studies reported
220 no significant change in KatG protein levels, while DpsA was upregulated during oxidative stress
221 (46). These findings suggest that transcriptional changes alone may not fully predict protein
222 abundance under stress conditions, and that translational regulation likely serves as an
223 additional rapid mechanism for fine-tuning protein levels during stress.
224
225 **Many small noncoding RNAs had ribosome occupancy.**
226 As expected, most ribosome footprints in our dataset corresponded to annotated coding
227 sequences. However, it was remarkable that several small noncoding RNAs (sRNAs), previously
228 identified by sRNA-seq (27), also exhibited ribosome occupancy. In total, 42 out of 56 sRNAs
229 detected in our RNA-seq dataset showed ribosome occupancy (TPM >10; Table S9), with 17 of
230 these sRNAs displaying differential ribosome occupancy or TE during oxidative stress (Table 3).
231
232 To investigate the coding potential of sRNAs with ribosome occupancy, we used several
233 computational approaches to identify putative small ORFs (smORFs; Fig. 2A). Public database
234 searches revealed nine annotated smORFs encoded by sRNAs (Fig. 2A). Of these, three have
235 been detected by mass spectrometry (MS) as reported in the Archaeal Proteome Project
236 database (64). Next, we used REPARATION (65), a tool designed to predict novel ORFs from
237 ribosome profiling data (53). Using our ribosome profiling dataset, REPARATION accurately
238 predicted 82% of all annotated proteins (Table S10), including 436 of 542 (80%) annotated
239 smORFs (≤100 amino acids). In addition, REPARATION predicted 194 novel genes (Table S11) of
240 which only seven encoded small proteins and one originated from a ribosome-associated sRNA
241 (Fig. 2A). While REPARATION predicted few smORFs within sRNAs, sequence-based tools such
242 as ORFfinder were overly permissive [Fig. 2A; (66)], often predicting ORFs in sRNAs even in the
243 absence of a stop codon within or around the sRNA sequence (Table S12).
244
245 These conflicting computational predictions, combined with empirical evidence for coding
246 potential for only 10 out of 42 sRNAs with ribosome occupancy (Fig. 2A), prompted further
247 investigation of the nature of the ribosome occupancy on sRNAs. To distinguish between true
248 translation and non-canonical ribosome association, we examined the ribosome footprint
249 length distribution. Footprint length distributions have previously been used to infer translation
250 states at a genome-wide level (52), and we applied this approach to individual sRNAs to assess
251 their coding potential.
252
253 **Size distributions of ribosome footprints revealed distinct patterns for coding and noncoding**
254 **genes.**
255 We analyzed ribosome footprint length distributions of coding genes, noncoding genes, and
256 sRNAs to assess the coding potential of ribosome-associated sRNAs. As expected, the
257 distribution of footprint lengths for coding genes - both at the level of individual genes - and
258 across the sum of all coding genes - was sharply enriched in footprints between 24 and 27
259 nucleotides (nt) in length (Fig. 2B). This was consistent with previous work identifying that the
260 characteristic footprint length for elongating ribosomes was 27 nt (52). In contrast, noncoding
261 genes, including rRNAs, SRP RNA, RNaseP RNA, and tRNAs, displayed distinct footprint length
262 distributions that were markedly different from those of coding genes (Fig. 2B).

To further explore sRNA coding potential, we performed clustering analysis based on the footprint length distributions of coding genes, noncoding genes, and sRNAs of interest. Clustering was optimized using the minimum number of clusters required to separate known coding genes from rRNAs and tRNAs. When clustering sRNAs with annotated smORFs (Fig. S5A), we observed that sRNAs with low total read counts did not consistently group with coding genes (Fig. S5B), indicating that sufficient read count is necessary to accurately infer coding potential. From this analysis, we determined that a minimum of 65 read counts across all biological replicates was required for reliable classification.

Using this threshold value, we found that 12 sRNAs clustered with known coding genes based on their footprint length distribution (Fig. 2B), seven of which corresponded to sRNAs with annotated smORFs. The high proportion of sRNAs with annotated smORFs included in the coding cluster supports the utility of footprint length distribution as a means of distinguishing coding from noncoding sRNAs, providing sufficient read coverage is available. However, we also identified 12 sRNAs ribosome-associated sRNAs that lacked both annotated smORFs and footprint length distributions consistent with coding genes.

Discovery of small proteins encoded by sRNA transcripts.

To validate predictions of coding sRNAs and assess whether predicted small proteins encoded by sRNAs could be detected, we used liquid chromatography tandem mass spectrometry (LC-MS/MS). This analysis included three biological replicates with and without oxidative stress treatment, the latter chosen to induce the expression of stress-responsive sRNAs. We sequentially passed cell lysates through centrifugal filters with 100 kDa and 30 kDa molecular cutoffs to deplete high molecular weight proteins (Fig. S6).

Our label-free quantitative differential expression analysis detected 2,095 proteins, filtered to 5% false discovery rate (FDR) and with at least two peptide spectrum matches (PSMs). This dataset represented 53% of the total proteome of *H. volcanii*, with a median protein sequence coverage of 59%, consistent with other high-quality MS datasets reported for this organism (64). As previously reported (67), centrifugal filtering is an imperfect method to enrich for small proteins, and indeed, the size distribution of the proteins we detected closely represented that of the full proteome (Fig. 3A). Notably, we did not detect any protein smaller than 25 amino acids, despite the existence of predicted smORFs as short as 10 amino acids (Fig. 3B). Nevertheless, we detected 235 smORFs (Fig. 3B) ranging from 31 to 100 amino acids in length, representing 40% of annotated smORFs (Table S13). Among these, seven smORFs were encoded within putative sRNAs, including four previously annotated (Fig. 2A; Table 1). For five out of these seven sRNA-encoded proteins, ribosome footprint length distributions clustered with those of known coding genes (Fig. 2B) and two smORFs, sRNA_93 and sRNA_KL, were highly conserved among haloarchaea. However, computational predictions, including sequence and structural homology searches, did not reveal functional annotations for these smORFs. Despite these findings, seven sRNAs with footprint length distributions consistent with coding genes lacked detectable protein-level evidence in our MS dataset.

307 To further investigate sRNAs with ribosome occupancy, we selected a subset for validation by
308 Western blot analysis (Table 2). This set included one sRNA with read counts below the
309 minimum threshold for clustering (sRNA_38), one sRNA not present in the coding cluster
310 (sRNA_83), three sRNAs within the coding cluster but not detected by MS (sRNA_20, sRNA_61,
311 and SHOxi), and two smORFs detected by MS (sRNA_KL, sRNA_93). Each selected sRNA was
312 tagged with a 3xFLAG epitope immediately downstream of the putative start codon and cloned
313 into *H. volcanii* on an overexpression plasmid (Fig. 3C). To preserve native regulatory elements,
314 150 bp upstream and 50 bp downstream of each sRNA were included. For sRNA_20, which
315 contained multiple putative ORFs, two start codons were tagged, including one corresponding
316 to a previously annotated protein. Western blot analysis confirmed the expression of both MS-
317 detected smORFs (sRNA_KL, sRNA_93), while no signal was observed for any of the other
318 tagged sRNAs (Fig. 3D). Despite having both expression level and ribosome occupancy
319 exceeding that of sRNA_KL and sRNA_93 (Table 2), no signal was detected for SHOxi and
320 sRNA_61. This strongly suggests that SHOxi and sRNA_61 function as noncoding RNAs.
321
322 Taken together, our combined LC-MS/MS and Western blot analyses identified seven smORFs
323 encoded by sRNAs, including three previously unannotated smORFs. However, several sRNAs -
324 most notably sRNA_61 and SHOxi - exhibited high ribosome occupancy without detectable
325 protein products, highlighting the complexity of interpreting ribosome profiling data and
326 suggesting potential regulatory or ribosome-associated noncoding functions.
327
328 **Ribosome-associated sRNAs may play regulatory roles during oxidative stress.**
329 We then focused on 17 stress-responsive sRNAs that had differential ribosome occupancy or TE
330 under oxidative stress conditions (Fig. 4A, Table 3). Among these, five sRNAs had annotated
331 smORFs, while the remaining 12 showed no evidence of coding potential. To further assess
332 their coding potential, we applied the ribosome footprint length clustering analysis described
333 earlier, this time using Ribo-seq data from oxidative stress-treated samples. Of the 12
334 unannotated sRNAs (with no evidence of coding potential), one failed to meet the minimum
335 read count threshold and was excluded from the analysis. Among the remaining 11, three
336 clustered with known coding genes, whereas nine did not (Fig. 4B). Given their lack of coding-
337 like ribosome footprint distributions, we hypothesized that these nine stress-responsive sRNAs
338 with high ribosome occupancy may play a regulatory role during oxidative stress. To investigate
339 their potential functional roles, we used a suite of *in silico* approaches. Notably, two sRNAs
340 were excluded from this analysis: SHOxi, which has been previously characterized as a
341 regulatory RNA (35), and sRNA_41, which is annotated as encoding a small protein.
342
343 We first performed BLASTn to assess the conservation of these noncoding stress-responsive
344 sRNAs. Five had homology to one or more halophilic species. However, for two of these, the
345 majority of homologous hits overlapped with an upstream gene on the opposite strand,
346 complicating the interpretation. The remaining two sRNAs had no detectable homology to
347 sequences in other species. We selected three sRNAs - sRNA_58, sRNA_77, and sRNA_83 - for
348 further analysis based on their conservation in at least one other species and the absence of
349 overlap with annotated genes.
350

351 We performed a multiple sequence alignment and predicted consensus secondary structures
352 for sRNA_58, sRNA_77, and sRNA_83 using LocARNA (68), incorporating all homologous
353 sequences identified in our BLASTn search. Each sRNA exhibited strong secondary structure
354 potential and high sequence conservation across species (Fig. 5A; Fig. S7), suggesting functional
355 relevance. To explore their regulatory role, we predicted putative mRNA targets using IntaRNA
356 [Fig. 5B; Tables S14-16; (69)] and determined which of those predicted targets had differential
357 ribosome occupancy or TE under oxidative stress (Fig. 5C, Table 4). sRNA_58 had the fewest
358 high-confidence predicted targets ($p < 0.01$), with only five out of 29 (17%) showing differential
359 ribosome occupancy or TE in response to oxidative stress. In contrast, sRNA_77 and sRNA_83
360 had a larger number of predicted high-confidence targets. Specifically, 13 out of 44 (30%)
361 putative mRNA targets for sRNA_83, and 15 out of 42 (36%) targets for sRNA_77 were
362 differentially translated in response to oxidative stress.
363
364 Collectively, of the eight sRNAs with differential ribosome occupancy or TE under oxidative
365 stress [excluding SHOxi, previously characterized (35)], five were conserved among halophilic
366 species. Two of these, sRNA_77 and sRNA_83, had numerous putative targets that exhibited
367 translational regulation during oxidative stress, suggesting they may play regulatory roles in the
368 stress response.
369
370 **sRNA knockouts have a similar phenotype to wild-type during oxidative stress.**
371 To explore the functional role of ribosome-associated sRNAs during oxidative stress, we
372 generated sRNA knockout strains for three sRNAs with a range of ribosome occupancy.
373 sRNA_24 represented low ribosome occupancy (TPM <10), sRNA_83 represented moderate
374 occupancy (50-100 TPM), and sRNA_20 represented high occupancy (>200 TPM). Knockouts
375 were generated as previously described (70) and whole genome sequencing confirmed the
376 complete deletion of the target sRNAs. Under oxidative stress conditions induced by H_2O_2
377 treatment, none of the knockout strains exhibited observable phenotypic differences compared
378 to the wild-type (WT) strain (Fig. S8A, B).
379
380 To identify putative regulatory targets for these sRNAs, we performed RNA-seq using three
381 biological replicates for each knockout strain and the WT strain exposed to oxidative stress,
382 along with non-stress WT controls, as previously described (35). The RNA-seq data were
383 analyzed, as described above, with significance cutoffs of adjusted p-value <0.05 and absolute
384 $\log_2$ fold change >1. No significantly differentially expressed genes were detected for sRNA_83
385 and sRNA_20 knockout strains when compared to the WT strain under oxidative stress (Fig.
386 S8C, D). However, we found 7 genes significantly upregulated for the sRNA_24 knockout strain
387 (Fig. S8E), which was further validated by qPCR (Fig. S8F). Three of these targets were members
388 of an operon involved in glycerol metabolism in *H. volcanii* [Table S17, (71)]. Remarkably,
389 genome analysis revealed that nine genes differentially regulated and with p-value <0.05 were
390 located immediately downstream of sRNA_24 locus (Fig. S8G, Table S17). None of these genes
391 were predicted as putative sRNA targets using IntaRNA, indicating a likely polar effect of the
392 sRNA gene deletion.
393

394 # Discussion

395 This study provides a comprehensive view of the translational landscape of the model archaeon
396 *H. volcanii* during oxidative stress by integrating RNA-seq and Ribo-seq analyses. While previous
397 studies in *H. volcanii* have reported changes in protein abundance under oxidative stress using
398 MS (46), such approaches cannot distinguish between transcriptional and translational
399 regulation. Furthermore, it is well established that transcript levels measured by RNA-seq often
400 correlate only modestly - and with high variability - with protein level determined by MS (72,
401 73), highlighting the complexity of processes that govern protein synthesis. To better
402 understand how gene expression is controlled at the level of translation, we used RNA-seq and
403 Ribo-seq to examine both ribosome occupancy and TE across the transcriptome.
404
405 Our analysis revealed that hundreds of genes exhibited differential TE in *H. volcanii* during
406 oxidative stress. Notably, we observed global downregulation of translation, particularly
407 affecting ribosomal proteins, suggesting a substantial reduction in *de novo* protein synthesis
408 under stress conditions. This translational repression is consistent with previous studies in *H.*
409 *volcanii* and *E. coli* under oxidative stress (27, 74, 75), as well as in *Halobacterium* NRC-1
410 following UV irradiation (76), all of which reported downregulation of translation-related genes.
411 This downregulation is thought to serve as a protective and energy-conserving strategy,
412 redirecting cellular resources toward damage repair and stress defense while minimizing
413 oxidative damage to the translation machinery (77). Similarly, in eukaryotic systems, stress-
414 induced translation arrest is well documented and often involves the formation of stress
415 granules containing translationally stalled complexes (40, 78, 79). Interestingly, a previous mass
416 spectrometry study in *H. volcanii* reported upregulation of several translation-related proteins,
417 including ribosomal proteins, in cells exposed to hypochlorite stress (46), highlighting potential
418 discrepancies between transcriptional, translational, and proteomic responses. However, a
419 study with *Halobacterium* NRC1 subjected to ionizing radiation (IR) addressed the sequential
420 nature of the cell's transcriptional (RNA-seq) and translational (proteomic) responses (80). The
421 study found a high level of correlation between mRNA and protein levels by temporally shifting
422 the protein level changes by 20 to 30 min, demonstrating the importance of the time
423 dimension.
424
425 In addition to translation-related genes, we observed downregulation of genes encoding
426 peroxidases and components of the tricarboxylic acid (TCA) cycle - findings that are consistent
427 with responses observed in *Deinococcus radiodurans* and *Halobacterium* NRC-1 following IR
428 (80-82). Because IR generates massive oxidative stress, suppression of general metabolism and
429 redox-active pathways may help cells limit further damage and maintain homeostasis. Taken
430 together, the divergence between RNA-seq, Ribo-seq, and MS datasets suggests that multiple
431 layers of regulation are employed to control gene expression during oxidative stress. Such
432 complex gene regulation has been documented in both eukaryotes and bacteria. For example,
433 cold shock protein in mammals (83), quorum sensing signals in *Agrobacterium tumefaciens* (84,
434 85), and the tryptophan operon in *E. coli* (86, 87) are all regulated at both the transcriptional
435 and translational levels. Similarly, in *H. volcanii*, the integration of transcriptional and
436 translational control likely enables a rapid and precise response to oxidative stress, allowing

437 selective synthesis of essential proteins while conserving energy by broadly reducing
438 translation.
439
440 Remarkably, we found that many sRNAs previously classified as noncoding (27) exhibited high
441 ribosome occupancy, suggesting that ribosome association may not be limited to actively
442 translated transcripts. Leveraging our Ribo-seq data, we analyzed ribosome footprint length
443 distribution and found that several of these sRNAs had footprint length distributions similar to
444 those of coding genes. A subset of these sRNAs were found to encode annotated smORFs, and
445 using MS, we identified seven small proteins encoded by sRNAs. Unfortunately, sequence or
446 structural homology searches did not provide insights into the potential functions of these
447 sRNA-encoded proteins. One exception is the small protein encoded in sRNA_KL, which has
448 previously been detected by both Ribo-seq and MS (53). This small protein contains a zinc
449 finger domain, and a deletion mutant showed increased growth on glycerol (88). It is important
450 to note that the ability to encode small proteins does not exclude these sRNAs from having
451 post-transcriptional regulatory roles. In bacteria, dual function sRNAs that both encode proteins
452 and act as regulatory sRNAs are well documented (89-91). Similar dual-function sRNAs have
453 been proposed in archaea, particularly under nitrogen starvation conditions (92). These findings
454 suggest that, as in other organisms (89, 93), *H. volcanii* may also use dual-function sRNAs,
455 especially in response to oxidative stress.
456
457 Ribo-seq is potentially a more sensitive method than MS for detecting smORFs (53, 92).
458 However, there is enduring concern that it may overestimate the number of translated sRNAs
459 (94, 95), making MS-based proteomics an important complementary approach to provide direct
460 protein-level evidence. In addition, analyzing ribosome footprint length distribution offers
461 another strategy to assess the coding potential of sRNAs. As discussed above, this analysis
462 successfully distinguished most coding genes and sRNAs with annotated smORFs from
463 noncoding genes. Nonetheless, this method was not accurate for all coding genes and requires
464 high read counts to reliably separate coding and noncoding transcripts.
465
466 We also identified several sRNAs with high ribosome occupancy that had no evidence of coding
467 potential. These sRNAs did not yield detectable protein even when putative ORFs were
468 individually tagged and probed by Western blotting. In contrast, smORFs detected by LC-MS
469 were also confirmed by Western blot, despite having lower ribosome occupancy. This
470 discrepancy may reflect the limitations in detecting low-abundance small proteins by MS or
471 Western blotting. For lowly expressed sRNAs, overexpression with an inducible promoter, as
472 previously shown (53), may be necessary for detection. Alternatively, sRNAs with high ribosome
473 occupancy and no evidence of coding potential may be functionally associated with ribosomes,
474 possibly directly interacting with them. Their association is unlikely to be an artefact of the
475 ribosome profiling protocol; although RNAs with secondary structure are generally resistant to
476 nuclease digestion, the small size of these sRNAs would prevent their co-sedimentation with
477 monosomes in a sucrose gradient. This suggests a specific association with ribosomes or
478 ribosome-bound mRNAs. Prior studies have reported the presence of sRNAs associated with
479 ribosomes in *H. volcanii* under stress conditions (96, 97). Sequencing and northern blotting of
480 sRNAs that co-purify with ribosomes identified a tRNA-derived fragment that binds the small

481 ribosome subunit, inhibiting peptide bond formation (96), as well as an intergenic sRNA that
482 interacts with the large subunit to regulate the translation of a specific mRNA (97).
483
484 Several ribosome-associated sRNAs lacking coding potential were also responsive to oxidative
485 stress, suggesting potential regulatory functions. These included SHOxi, which binds to and
486 destabilizes malic enzyme transcripts, enhancing cell survival during oxidative stress (35), thus
487 arguing against this sRNA being a nonfunctional *de novo* gene intermediate. Importantly, our
488 RNA-seq and Ribo-seq experiments were performed with four biological replicates each, and
489 the ribosome-associated sRNAs discussed here consistently showed high ribosome
490 occupancies. Deletion of three such sRNAs did not result in a growth phenotype under oxidative
491 stress and caused little to no change in the expression level of other genes. This suggests that
492 these sRNAs may not modulate transcript stability directly, unlike some well-characterized
493 sRNAs in both bacteria (32, 98, 99) and archaea (100, 101). For example, in *H. volcanii*, SHOxi
494 destabilized its mRNA target through complementary base pairing (35). However, as observed
495 in bacterial systems (102, 103), deletion of a single sRNA may be insufficient to observe its
496 regulatory function. Targeted knockout of multiple stress-responsive, ribosome-associated
497 sRNAs may therefore be necessary to fully elucidate their role during oxidative stress. Taken
498 together, our findings suggest that several oxidative stress-associated sRNAs in *H. volcanii* are
499 closely associated with ribosomes but do not affect mRNA stability. We hypothesize they
500 regulate translation directly through interaction with the ribosome or ribosome-bound mRNAs.
501
502 Using RNA-seq and Ribo-seq in a model archaeon, we demonstrated global and targeted
503 translation regulation in response to oxidative stress. We also identified a class of untranslated,
504 ribosome-associated sRNAs likely involved in translational regulation under oxidative stress.
505 While the precise mechanisms of action remain to be elucidated, this study highlights the
506 complexity of translational regulation in archaea and underscore the multifaceted architecture
507 of stress-responsive regulatory networks.
508

509 # Materials and Methods

510 **Cell culturing and oxidative stress treatment**

511 *Haloferax volcanii* DS2 strain H98 (70) was grown in liquid Hv-YPC (70) supplemented with 40
512 mg/mL thymidine at 42°C, with shaking, to OD >0.5. Cultures were diluted into fresh media to
513 an OD of 0.01 and grown to OD 0.4-0.6. For oxidative stress treatment, cultures were incubated
514 with 2mM H_2O_2 for one hour at 42°C with shaking, as previously described (27).

515 **Ribosome profiling**

516 Ribo-seq was performed as previously described (52, 104). In brief, cultures were flash frozen in
517 liquid nitrogen and lysed by cryogenic mill, using 55 g of frozen culture and 100 µg/mL of
518 anisomycin. Ribosomes were collected by ultracentrifugation on a 1 M sucrose cushion using a
519 Ti45 rotor at 185,511x*g* (40,000 rpm) for three hours at 4°C. Polysomes were digested using
520 MNase and separated using a 10-50% sucrose gradient (Fig. S9A). RNA from monosome
521 fractions was isolated with Trizol LS reagent, followed by size selection (Fig. S9B), and
522 generation of libraries for high-throughput sequencing (Fig. S9C, D). Libraries were sequenced
523 by Novogene (150 bp, paired-end reads, NovaSeq).

524 **RNA-seq**
525 RNA-seq libraries were prepared using 20 mL of culture pelleted by centrifugation. RNA
526 extraction was performed as previously described (27) using a Quick-RNA Miniprep kit (Zymo).
527 rRNA was depleted using 2.5 µg of DNase-treated RNA and the Ribo-Zero rRNA removal kit for
528 bacteria (Illumina). The SMARTer Stranded RNA-Seq kit (Takara Bio) was used to prepare the
529 libraries with 100 ng RNA, dual-index primers, and 12 PCR cycles. Libraries were sequenced by
530 Novogene (150 bp, paired-end reads, NovaSeq). For knockout strains, RNA was prepared as
531 described above, using 3 replicates per strain. All strains were treated with H_2O_2, with 3
532 replicates of untreated WT as controls. Library preparation and sequencing were performed by
533 SeqCenter in Pittsburgh, PA (150 bp, paired-end reads, NovaSeq X plus) using Illumina's
534 Stranded Total RNA Prep Ligation with Ribo-Zero Plus kit and custom probes.
535 **Analysis of sequencing data**
536 Demultiplexed reads provided by Novogene and SeqCenter were analyzed using only forward
537 reads for Ribo-seq libraries and both reads for RNA-seq libraries. For full analysis details, see
538 Table S18. Adapters were trimmed using Trim Galore [(105),
539 https://github.com/FelixKrueger/TrimGalore] and reads were aligned to rRNA genes using
540 Bowtie (106). Unaligned reads (those not aligning to rRNA) were written to a new file and used
541 for genome alignment, which was performed using Bowtie and the *H. volcanii* DS2 genome
542 assembly ASM2568v1 from NCBI (49). Samtools (107) was used to generate bam and sorted
543 bam files. Coverage and depth were calculated using samtools and bedtools. Average depth per
544 chromosome was calculated using a custom Python script. TPM were calculated using StringTie
545 (108), with a provided reference annotation file (gff from NCBI Refseq assembly
546 GCF_000025685.1 downloaded March 2023 with added entries for sRNAs). Read counts were
547 calculated using featureCounts (109). See Tables S19, S20, and S21 for statistical summaries of
548 all analyses.
549 **Differential expression and TE analysis**
550 Differential expression was determined using DESeq2 (110). For RNA-seq and Ribo-seq data, the
551 variable of interest was experimental condition. For TE, the ratio between Ribo-seq and RNA-
552 seq was used, in addition to two variables of interest: sample (RNA-seq or Ribo-seq) and
553 experimental condition. For full details, see Table S18.
554 **Characterization of significant genes**
555 The number of leaderless genes was determined using published data that characterized 1851
556 annotated genes as leadered or leaderless (111). 68% of genes with differential TE were
557 uncharacterized and therefore not considered in calculations for the percent of leaderless
558 genes. Custom Python scripts were used to calculate percent of leaderless genes, codon
559 frequencies, and amino acid frequencies. Heatmaps were generated using R. The STRING
560 database [web version 12.0; (58)] was used to predict interactions and to determine KEGG
561 enrichments with default settings and MCL clustering. Gene interaction predictions are based
562 on evidence including genomic proximity, experimental data and co-expression of homologs,
563 association in curated databases, and text mining of abstracts from published literature. 84% of
564 genes with differential TE were successfully mapped to the STRING database. The PANTHER
565 database (web version 19.0) was used to generate a generic mapping file (57, 112) for the *H.*
566 *volcanii* DS2 protein fasta file downloaded from NCBI. Overrepresentation tests were
567 conducted using Fisher's test and FDR correction.

568 **smORF prediction**
569 For ORF prediction using the web version of Open Reading Frame Finder [ORFfinder, NCBI;
570 (66)], a minimal length of 30 nt and alternative initiation codons were allowed. For ORF
571 prediction using Ribo-seq data, an adapted version of REPARATION (65), using blast instead of
572 USEARCH (https://github.com/RickGelhausen/REPARATION_blast) was used. For option details,
573 see Table S18. A custom python script compared and combined predictions with and without
574 Shine-Dalgarno. Predicted genes were visualized using IGV, and a manual scan was conducted
575 to compare overlap between replicates for control or oxidative stress treatment. Predicted
576 genes were required to be present in at least 3 biological replicates. Novel gene lists for control
577 and stress samples were then combined.
578 **Footprint distribution clustering**
579 Lengths of reads aligning to individual genes were obtained using a custom Bash script,
580 followed by analysis using R to generate heatmaps. Clustering was performed using the
581 pheatmap (https://github.com/raivokolde/pheatmap) package with default settings and the
582 minimum number of clusters required to separate rRNA from known coding genes in control
583 samples.
584 **Mass spectrometry sample preparation**
585 Samples for mass spectrometry were prepared using 600 mL cultures from three replicates; half
586 of the culture was used for control samples and the other half was treated with H_2O_2. Cells
587 were pelleted by centrifugation then resuspended in 8 mL lysis buffer (2 M NaCl, 8 M urea, 0.1
588 M Tris-Cl, 10 mM DTT) and flash frozen. Resuspension was ground in a cryogenic mill (SPEX
589 6870) with a 1 minute pre-cool, then 8 cycles of alternating 1 minute of run time and 1 minute
590 of cool time, at a rate of 8 cycles/second. The thawed lysate was spun twice at 15000 x*g* for 15
591 minutes at 4°C. Lysis buffer was added to a volume of 10 mL, then filtered through a 0.2-micron
592 syringe filter and brought to a final volume of 12 mL with lysis buffer. Size selection was
593 performed by centrifugation in 100K MWCO filters (Pall) at 5000 x*g* for 2 hours at room
594 temperature, then centrifugation in 30K MWCO filters (Pall) at 5000 x*g* for 45 minutes at room
595 temperature. Iodoacetamide was added to a final concentration of 54 mM and incubated for 45
596 minutes in the dark at room temperature, followed by addition of 11.1% of volume of
597 trichloroacetic acid. Samples were flash frozen, then incubated at 4°C overnight. Samples were
598 centrifuged at 20000 x*g* for 30 minutes at 4°C and supernatant was removed. Pellets were
599 washed twice with acetone, air-dried for 10 minutes, then resuspended in 50 µL of 8 M urea in
600 phosphate-buffered saline (PBS), pH 7.4 and quantified using the Qubit Protein Assay kit. 30 µg
601 of total protein in 200 µL of 2 M urea in PBS, pH 7.4 were digested with trypsin and prepared
602 for MS as previously described (113).
603 **Mass spectrometry acquisition**
604 Chromatographic separation of protein digests was carried out as previously described (114),
605 injecting 1 µg of protein per sample.
606 **Mass spectrometry data analysis**
607 The Proteome Discoverer (PD) Software Suite v2.4, Minora Algorithm (ThermoFisher) was used
608 to process mass spectra and perform Label Free Quantification (LFQ), comparing control and
609 stress samples with default settings for all analysis nodes except where specified. Data were
610 searched against the *H. volcanii* DS2 proteome fasta file from Uniprot (entry UP000008243,
611 organism ID 309800; downloaded January 2023). The reference fasta file was appended with

612 additional sequences for putative smORFs. For peptide identification, the Proteome Discoverer
613 Sequest HT node was selected for a tryptic search allowing up to 2 missed cleavages. A
614 precursor mass tolerance of 10 ppm was used for the MS1 level, and a fragment ion tolerance
615 of 0.02 was set at the MS2 level. Methionine oxidation and N-terminus acetylation were
616 allowed as dynamic modifications, with carbamidomethylation on cysteines defined as a static
617 modification. Protein abundance ratio data were exported using a three-level hierarchy
618 (protein > peptide group > consensus features). A minimum of 2 PSMs and maximum FDR of 5%
619 were required to determine detection of novel small proteins. See Table S22 for statistical
620 summaries.

621 **Generating tagged sRNAs**

622 sRNA regions (including at minimum 150 bp upstream and 50 bp downstream) were amplified
623 from genomic DNA and cloned into pTA1300 using *Kas*I and *Bam*HI. Ligation products were
624 transformed into DH5α competent cells (NEB), followed by plasmid extraction (QIAprep spin
625 miniprep kit) and verification by Sanger sequencing (GENEWIZ, Azenta). A 3xFLAG tag was
626 added after the predicted start codon using Q5 site-directed mutagenesis (NEB). Purified
627 plasmids were transformed into *H. volcanii* as previously described (115), using the lab strain
628 H98.

629 **Western blots**

630 25 mL of culture were pelleted by centrifugation at 10,000 x*g* for 6 minutes at 4°C. Pellets were
631 resuspended in 1 mL lysis buffer (50 mM Tris-HCl pH 7.5, 2 M urea, 0.2% SDS, 0.1 mg/mL EDTA-
632 free protease inhibitor cocktail (Roche)) and lysed with sterile glass beads (116). Protein
633 concentration was quantified using the Qubit Protein Assay kit. Proteins (10-100 µg total) were
634 separated on a 4-15% stain free acrylamide gel (BioRad), transferred to a nitrocellulose
635 membrane, and incubated with anti-Flag monoclonal antibodies conjugated with alkaline
636 phosphatase (1:10,000 dilution; Sigma cat no. A9469), as previously described (116). The
637 antibody:protein complexes were visualized using 0.25 mM CDP-Star Substrate (Tropix) with 1x
638 Nitro-Block-II Enhancer (Invitrogen) and the BioRad ChemiDoc Imager.

639 **sRNA in silico tools**

640 Web versions of nucleotide BLAST (117), IntaRNA (69, 118), and LocARNA (68) were used with
641 default settings.

642 **Generating knockouts**

643 Knockout strains were generated using the established protocol for *H. volcanii* (70). For
644 sRNA_83, a knockout plasmid was constructed by amplifying upstream and downstream
645 flanking regions from genomic DNA and cloning into pTA131 using *Hind*III, *Xba*I, and *Eco*RI.
646 Knockout plasmids for sRNA_20 and sRNA_24 were generated by Azenta, with upstream and
647 downstream flanking regions cloned into pTA131 using *Hind*III and *Xba*I. Knockout plasmids
648 were transformed into *H. volcanii* (115), strain H98, followed by selection for pop-in (uracil
649 selection) and pop-out (5-FOA selection). Whole genome sequencing of successful pop-outs
650 was performed by Plasmidsaurus using Oxford Nanopore Technology with custom analysis. For
651 ΔsRNA_83 and ΔsRNA_24, no additional mutations were identified. For ΔsRNA_20, two
652 additional point mutations were detected (C->G at position 50,650 in HVO_RS02135; A->G at
653 position 1,284,523 in HVO_RS11505).

654 **Knockout phenotyping**

To assess survival during acute oxidative stress, 3 replicates of WT and mutant strains were grown as described above in a total volume of 20 mL. 50 µL of culture were plated, and remaining culture was treated with H_2O_2. Cultures were plated on YPC with thymidine and incubated at 42°C for 4 days. Colonies were counted and used to calculate CFUs/mL and percent survival. To assess survival during chronic oxidative stress, 3 replicates of WT and mutant strains were grown as described above. Cultures were diluted into fresh media to an OD of 0.02 and treated with various H_2O_2 concentrations. Cultures were transferred to 100-well plates (250 µL/well) and grown in a Bioscreen C Pro for 42 hours at 42°C with shaking (normal speed, max amplitude, orbital). Absorbance measurements were taken every six hours. Data were plotted using R.

qPCR

Samples for qPCR were prepared using 40 mL cultures from 3 replicates; half used for control samples and half treated with H_2O_2. Cells were harvested and RNA was extracted as described for RNA-seq library preparation. Conversion to cDNA was performed using a Superscript RT III kit (Invitrogen) with random hexamers. qPCR was conducted in 48-well plates with PowerUp™ SYBR™ Green Master Mix (Applied Biosystems, A25742) using the StepOne™ Real-Time PCR System with standard conditions and annealing temperature of 60°C (for primers, see Table S23). Fold change was determined by the Livak method (119).

Data availability

RNA-seq reads, ribosome profiling reads, and annotation files are available on NCBI GEO: GSE293312 (RNA-seq) and GSE293326 (Ribo-seq). The mass spectrometry proteomics data have been deposited to the ProteomeXchange Consortium via the PRIDE (120) partner repository with the dataset identifier PXD062323 and 10.6019/PXD062323. Data analysis scripts are available on GitHub: https://github.com/diruggiero-lab/sRNAs.

Acknowledgements

We thank Dr. Cesar Perez-Fernandez, Dr. Diego Gelsinger, and Frank Liu for experimental advice and helpful discussions. We thank Matthew F. Isada for extensive manuscript editing and helpful discussions. This work was supported by US National Science Foundation grants MCB-2034271 and MCB-57951. We would also like to thank the NSF Division of Molecular and Cellular Biology for a CAREER grant (Grant No. 2045844) and NIH/NIGMS for a New Innovator Award (No. DP2-GM140926) both to SDF. SDF further acknowledges support from the Camille & Henry Dreyfus Foundation and the Sloan Foundation. HMM is thankful for the Chemistry-Biology Interface Program training grant (Grant No. NIH-T32GM080189-13).

E.D.: Conceptualization, Methodology, Investigation – RNA-seq, Ribo-seq, mass spectrometry sample preparation, Western blots, knockout phenotyping, Formal analysis – analysis of sequencing data, footprint distribution analysis, Visualization, Writing – original draft, Writing – review & editing; H.M.M: Investigation – mass spectrometry sample preparation, mass spectrometry data acquisition, Formal analysis – mass spectrometry data analysis, Writing – review & editing; S.R.C: Formal analysis – DESeq2 analysis for all datasets; A.K.: Investigation – construction of tagged sRNA constructs and sRNA knockout strains, qPCR analysis; B.Y.H.H.:

698 Investigation – construction of tagged sRNA constructs; S.D.F.: Methodology, Writing – review
699 & editing; J.D.: Conceptualization, Methodology, Funding acquisition, Writing – review &
700 editing, Supervision. All authors read and approved the final manuscript.
701

702 References

703 1. Cabiscol Catalā E, Tamarit Sumalla, J, Ros Salvador, J. 2000. Oxidative stress in bacteria and
704 protein damage by reactive oxygen species. Int Microbiol 3:3-8.

705 2. Seixas AF, Quendera, AP, Sousa, JP, Silva, AFQ, Arraiano, CM, Andrade, JM. 2022. Bacterial
706 response to oxidative stress and RNA oxidation. Front Genet 12: 821535.

707 3. Ezraty B, Gennaris, A, Barras, F, Collet, J. 2017. Oxidative stress, protein damage and repair in
708 bacteria. Nat Rev Microbiol 15:385–396.

709 4. Maezato Y, Blum, P. 2012. Survival of the fittest: Overcoming oxidative stress at the extremes
710 of acid, heat and metal. Life 2:242.

711 5. Farrugia G, Balzan, R. 2012. Oxidative stress and programmed cell death in yeast. Front Oncol
712 2:64.

713 6. Jelic MD, Mandic, AD, Maricic, SM, Srdjenovic, BU. 2021. Oxidative stress and its role in
714 cancer. J Cancer Res Ther 17:22–28.

715 7. Teleanu DM, Niculescu, A, Lungu, II, Radu, CI, Vladâcenco, O, Roza, E, Costăchescu, B,
716 Grumezescu, AM, Teleanu, RI. 2022. An overview of oxidative stress, neuroinflammation, and
717 neurodegenerative diseases. Int J Mol Sci 23:5938.

718 8. Steven S, Frenis, K, Oelze, M, Kalinovic, S, Kuntic, M, Bayo Jimenez, MT, Vujacic-Mirski, K,
719 Helmstädter, J, Kröller-Schön, S, Münzel, T, Daiber, A. 2019. Vascular inflammation and
720 oxidative stress: Major triggers for cardiovascular disease. Oxid Med Cell Longev 2019:7092151.

721 9. Johnson LA, Hug, LA. 2019. Distribution of reactive oxygen species defense mechanisms
722 across domain bacteria. Free Radic Biol Med 140:93–102.

723 10. Sato Y, Kameya, M, Fushinobu, S, Wakagi, T, Arai, H, Ishii, M, Igarashi, Y. 2012. A novel
724 enzymatic system against oxidative stress in the thermophilic hydrogen-oxidizing bacterium
725 *Hydrogenobacter thermophilus*. Plos One 7:e34825.

726 11. Cannio R, D'angelo, A, Rossi, M, Bartolucci, S. 2000. A superoxide dismutase from the
727 archaeon *Sulfolobus solfataricus* is an extracellular enzyme and prevents the deactivation by
728 superoxide of cell-bound proteins. Eur J Biochem 267:235–243.

729 12. Takao M, Oikawa, A, Yasui, A. 1990. Characterization of a superoxide dismutase gene from
730 the archaebacterium *Methanobacterium thermoautotrophicum*. Arch Biochem Biophys
731 283:210–216.

732 13. Jeon S, Ishikawa, K. 2002. Identification and characterization of thioredoxin and thioredoxin
733 reductase from *Aeropyrum pernix* K1. Eur J Biochem 269:5423–5430.

734 14. Dea S, Miroslav, R. 2011. Oxidative stress resistance in *Deinococcus radiodurans*. Microbiol
735 Mol Biol Rev 75:133–191.

736 15. Matarredona L, Camacho, M, Zafrilla, B, Bravo-Barrales, G, Esclapez, J, Bonete, M. 2021. The
737 survival of *Haloferax mediterranei* under stressful conditions. Microorganisms 9:336.

738 16. Robinson CK, Webb, K, Kaur, A, Jaruga, P, Dizdaroglu, M, Baliga, NS, Place, A, DiRuggiero, J.
739 2011. A major role for nonenzymatic antioxidant processes in the radioresistance of
740 *Halobacterium salinarum*. J Bacteriol 193:1653–1662.

741 17. Webb KM, Yu, J, Robinson, CK, Noboru, T, Lee, YC, DiRuggiero, J. 2013. Effects of
742 intracellular Mn on the radiation resistance of the halophilic archaeon *Halobacterium*
743 *salinarum*. Extremophiles 17:485–497.

744 18. Eme L, Spang, A, Lombard, J, Stairs, CW, Ettema, TJG. 2017. Archaea and the origin of
745 eukaryotes. Nat Rev Microbio 15:711–723.

746 19. Phung DK, Etienne, C, Batista, M, Langendijk-Genevaux, P, Moalic, Y, Laurent, S, Liuu, S,
747 Morales, V, Jebbar, M, Fichant, G, Bouvier, M, Flament, D, Clouet-d'Orval, B. 2020. RNA
748 processing machineries in archaea: The 5'-3' exoribonuclease aRNase J of the β-CASP family is
749 engaged specifically with the helicase ASH-Ski2 and the 3'-5' exoribonucleolytic RNA exosome
750 machinery. Nucleic Acids Res 48:3832–3847.

751 20. Brochier-Armanet C, Forterre, P, Gribaldo, S. 2011. Phylogeny and evolution of the archaea:
752 One hundred genomes later. Curr Opin Microbiol 14:274–281.

753 21. Řezanka T, Kyselová, L, Murphy, DJ. 2023. Archaeal lipids. Prog Lipid Res 91:101237.

754 22. Humbard MA, Miranda, HV, Lim, J, Krause, DJ, Pritz, JR, Zhou, G, Chen, S, Wells, L, Maupin-
755 Furlow, JA. 2010. Ubiquitin-like small archaeal modifier proteins (SAMPs) in *Haloferax volcanii*.
756 Nature 463:54–60.

757 23. Nunoura T, Takaki, Y, Kakuta, J, Nishi, S, Sugahara, J, Kazama, H, Chee, G, Hattori, M, Kanai,
758 A, Atomi, H, Takai, K, Takami, H. 2010. Insights into the evolution of archaea and eukaryotic
759 protein modifier systems revealed by the genome of a novel archaeal group. Nucleic Acids Res
760 39:3204–3223.

761 24. Haque RU, Paradisi, F, Allers, T. 2020. *Haloferax volcanii* for biotechnology applications:
762 Challenges, current state and perspectives. Appl Microbiol Biotechnol 104:1371–1382.

763 25. Pastor MM, Darnell, CL, Vreugdenhil, A, Schmid, AK. 2024. Rapid rewiring of an archaeal
764 transcription factor function via flexible cis-trans interactions. bioRxiv 2024.11.20.624553.

765 26. Sharma K, Gillum, N, Boyd, JL, Schmid, A. 2012. The RosR transcription factor is required for
766 gene expression dynamics in response to extreme oxidative stress in a hypersaline-adapted
767 archaeon. BMC Genomics 13:351–351.

768 27. Gelsinger DR, DiRuggiero, J. 2018. Transcriptional landscape and regulatory roles of small
769 noncoding RNAs in the oxidative stress response of the haloarchaeon *Haloferax volcanii*. J
770 Bacteriol 200:e00779–17.

771 28. Lease RA, Smith, D, McDonough, K, Belfort, M. 2004. The small noncoding DsrA RNA is an
772 acid resistance regulator in *Escherichia coli*. J Bacteriol 186:6179–6185.

773 29. Majdalani N, Chen, S, Murrow, J, St John, K, Gottesman, S. 2001. Regulation of RpoS by a
774 novel small RNA: The characterization of RprA. Mol Microbiol 39:1382–1394.

775 30. Massé E, Gottesman, S. 2002. A small RNA regulates the expression of genes involved in
776 iron metabolism in *Escherichia coli*. Proc Nat Acad Sci U S A 99:4620–4625.

777 31. Delihas N, Forst, S. 2001. MicF: An antisense RNA gene involved in response of E*scherichia*
778 *coli* to global stress factors11Edited by D. draper. J Mol Biol 313:1–12.

779 32. Lalaouna D, Baude, J, Wu, Z, Tomasini, A, Chicher, J, Marzi, S, Vandenesch, F, Romby, P,
780 Caldelari, I, Moreau, K. 2019. RsaC sRNA modulates the oxidative stress response of
781 *Staphylococcus aureus* during manganese starvation. Nucleic Acids Res 47:9871–9887.

782 33. Altuvia S, Weinstein-Fischer, D, Zhang, A, Postow, L, Storz, G. 1997. A small, stable RNA
783 induced by oxidative stress: Role as a pleiotropic regulator and antimutator. Cell 90:43–53.

784 34. Chen Y, Xue, D, Sun, W, Han, J, Li, J, Gao, R, Zhou, Z, Zhang, W, Chen, M, Lin, M, Wang, J,
785 Zuo, K. 2019. sRNA OsiA stabilizes catalase mRNA during oxidative stress response of
786 *Deincoccus radiodurans* R1. Microorganisms 7:422.

787 35. Gelsinger DR, Reddy, R, Whittington, K, Debic, S, DiRuggiero, J. 2021. Post-transcriptional
788 regulation of redox homeostasis by the small RNA SHOxi in haloarchaea. RNA Biol 18:1867–
789 1881.

790 36. Halbeisen RE, Gerber, AP. 2009. Stress-dependent coordination of transcriptome and
791 translatome in yeast. PLOS Biology 7:e1000105.

792 37. Picard F, Loubière, P, Girbal, L, Cocaign-Bousquet, M. 2013. The significance of translation
793 regulation in the stress response. BMC Genomics 14:588.

794 38. Kuhn KM, DeRisi, JL, Brown, PO, Sarnow, P. 2001. Global and specific translational
795 regulation in the genomic response of *Saccharomyces cerevisiae* to a rapid transfer from a
796 fermentable to a nonfermentable carbon source. Mol Cell Biol 21:916–927.

797 39. Melamed D, Pnueli, L, Arava, Y. 2008. Yeast translational response to high salinity: Global
798 analysis reveals regulation at multiple levels. RNA 14:1337–1351.

799 40. Gerashchenko MV, Lobanov, AV, Gladyshev, VN. 2012. Genome-wide ribosome profiling
800 reveals complex translational regulation in response to oxidative stress. Proc Natl Acad Sci U S A
801 109:17394–17399.

802 41. Benelli D, Marzi, S, Mancone, C, Alonzi, T, la Teana, A, Londei, P. 2008. Function and
803 ribosomal localization of aIF6, a translational regulator shared by archaea and eukarya. Nucleic
804 Acids Res 37:256–267.

805 42. Jäger D, Pernitzsch, SR, Richter, AS, Backofen, R, Sharma, CM, Schmitz, RA. 2012. An
806 archaeal sRNA targeting cis - and trans -encoded mRNAs via two distinct domains. Nucleic Acids
807 Res 40:10964–10979.

808 43. Prasse D, Ehlers, C, Backofen, R, Schmitz, RA. 2013. Regulatory RNAs in archaea: First target
809 identification in methanoarchaea. Biochem Soc Trans 41:344–349.

810 44. Altuvia S, Zhang, A, Argaman, L, Tiwari, A, Storz, G. 1998. The *Escherichia coli* OxyS
811 regulatory RNA represses *fhlA* translation by blocking ribosome binding. Embo J 17:6069–6075;
812 6075.

813 45. Jevtić Ž, Stoll, B, Pfeiffer, F, Sharma, K, Urlaub, H, Marchfelder, A, Lenz, C. 2019. The
814 response of *Haloferax volcanii* to salt and temperature stress: A proteome study by label-free
815 mass spectrometry. Proteomics 19:1800491.

816 46. McMillan LJ, Hwang, S, Farah, RE, Koh, J, Chen, S, Maupin-Furlow, JA. 2018. Multiplex
817 quantitative SILAC for analysis of archaeal proteomes: A case study of oxidative stress
818 responses. Environ Microbiol 20:385–401.

819 47. Soborowski AL, Hackley, RK, Hwang, S, Zhou, G, Dulmage, K, Schönheit, P, Daniels, C, Bisson-
820 Filho, AW, Marchfelder, A, Maupin-Furlow, JA, Allers, T, Schmid, AK. 2024. Genomic re-
821 sequencing reveals mutational divergence across genetically engineered strains of model
822 archaea. bioRxiv 2024.08.08.607208.

823 48. Hawkins M, Malla, S, Blythe, MJ, Nieduszynski, CA, Allers, T. 2013. Accelerated growth in the
824 absence of DNA replication origins. Nature 503:544–547.

825 49. Hartman AL, Norais, C, Badger, JH, Delmas, S, Haldenby, S, Madupu, R, Robinson, J, Khouri,
826 H, Ren, Q, Lowe, TM, Maupin-Furlow, J, Pohlschroder, M, Daniels, C, Pfeiffer, F, Allers, T, Eisen,
827 JA. 2010. The complete genome sequence of *Haloferax volcanii* DS2, a model archaeon. PLoS
828 One 5:e9605.

829 50. Pohlschroder M, Schulze, S. 2019. *Haloferax volcanii*. Trends Microbiol 27:86–87.

830 51. Pérez-Arnaiz P, Dattani, A, Smith, V, Allers, T. 2020. *Haloferax volcanii*-a model archaeon for
831 studying DNA replication and repair. Open Biol 10:200293.

832 52. Gelsinger DR, Dallon, E, Reddy, R, Mohammad, F, Buskirk, AR, DiRuggiero, J. 2020. Ribosome
833 profiling in archaea reveals leaderless translation, novel translational initiation sites, and
834 ribosome pausing at single codon resolution. Nucleic Acids Res 48:5201–5216.

835 53. Hadjeras L, Bartel, J, Maier, L, Maaß, S, Vogel, V, Svensson, SL, Eggenhofer, F, Gelhausen, R,
836 Müller, T, Alkhnbashi, OS, Backofen, R, Becher, D, Sharma, CM, Marchfelder, A. 2023. Revealing
837 the small proteome of *Haloferax volcanii* by combining ribosome profiling and small-protein
838 optimized mass spectrometry. Microlife 4:uqad001.

839 54. Ingolia I, Ghaemmaghami, G, Newman, N, Weissman, W. 2009. Genome-wide analysis *in*
840 *vivo* of translation with nucleotide resolution using ribosome profiling. Science 324:218–223.

841 55. Kramer P, Gäbel, K, Pfeiffer, F, Soppa, J. 2014. *Haloferax volcanii*, a prokaryotic species that
842 does not use the Shine Dalgarno mechanism for translation initiation at 5'-UTRs. PloS One
843 9:e94979.

844 56. Mi H, Muruganujan, A, Casagrande, JT, Thomas, PD. 2013. Large-scale gene function
845 analysis with the PANTHER classification system. Nat Protoc 8:1551–1566.

846 57. Mi H, Muruganujan, A, Huang, X, Ebert, D, Mills, C, Guo, X, Thomas, PD. 2019. Protocol
847 update for large-scale genome and gene function analysis with the PANTHER classification
848 system (v.14.0). Nat Protoc 14:703–721.

849 58. Szklarczyk D, Kirsch, R, Koutrouli, M, Nastou, K, Mehryary, F, Hachilif, R, Gable, AL, Fang, T,
850 Doncheva, NT, Pyysalo, S, Bork, P, Jensen, LJ, von Mering, C. 2023. The STRING database in
851 2023: Protein-protein association networks and functional enrichment analyses for any
852 sequenced genome of interest. Nucleic Acids Res 51:D638–D646.

853 59. Mondragon P, Hwang, S, Kasirajan, L, Oyetoro, R, Nasthas, A, Winters, E, Couto-Rodriguez,
854 RL, Schmid, A, Maupin-Furlow, JA. 2022. TrmB family transcription factor as a thiol-based
855 regulator of oxidative stress response. mBio 13:e0063322–22.

856 60. Llorca MG, Martínez-Espinosa, RM. 2022. Assessment of *Haloferax mediterranei* genome in
857 search of copper-molecular machinery with potential applications for bioremediation. Front
858 Microbiol 13:895296.

859 61. Liao Y, Williams, TJ, Ye, J, Charlesworth, J, Burns, BP, Poljak, A, Raftery, MJ, Cavicchioli, R.
860 2016. Morphological and proteomic analysis of biofilms from the antarctic archaeon,
861 *Halorubrum lacusprofundi*. Sci Rep 6:37454.

862 62. Reindel S, Anemüller, S, Sawaryn, A, Matzanke, BF. 2002. The DpsA-homologue of the
863 archaeon *Halobacterium salinarum* is a ferritin. Biochim Biophys Acta 1598:140–146.

864 63. Zeth K, Offermann, S, Essen, L, Oesterhelt, D. 2004. Iron-oxo clusters biomineralizing on
865 protein surfaces: Structural analysis of *Halobacterium salinarum* DpsA in its low- and high-iron
866 states. Proc Natl Acad Sci U S A 101:13780–13785.

867 64. Schulze S, Adams, Z, Cerletti, M, De Castro, R, Ferreira-Cerca, S, Fufezan, C, Giménez, MI,
868 Hippler, M, Jevtic, Z, Knüppel, R, Legerme, G, Lenz, C, Marchfelder, A, Maupin-Furlow, J, Paggi,
869 RA, Pfeiffer, F, Poetsch, A, Urlaub, H, Pohlschroder, M. 2020. The archaeal proteome project
870 advances knowledge about archaeal cell biology through comprehensive proteomics. Nat
871 Commun 11:3145.

872 65. Ndah E, Jonckheere, V, Giess, A, Valen, E, Menschaert, G, Van Damme, P. 2017.
873 REPARATION: Ribosome profiling assisted (re-)annotation of bacterial genomes. Nucleic Acids
874 Res 45:e168.

875 66. Sayers EW, Barrett, T, Benson, DA, Bolton, E, Bryant, SH, Canese, K, Chetvernin, V, Church,
876 DM, DiCuccio, M, Federhen, S, Feolo, M, Fingerman, IM, Geer, LY, Helmberg, W, Kapustin, Y,
877 Landsman, D, Lipman, DJ, Lu, Z, Madden, TL, Madej, T, Maglott, DR, Marchler-Bauer, A, Miller,
878 V, Mizrachi, I, Ostell, J, Panchenko, A, Phan, L, Pruitt, KD, Schuler, GD, Sequeira, E, Sherry, ST,
879 Shumway, M, Sirotkin, K, Slotta, D, Souvorov, A, Starchenko, G, Tatusova, TA, Wagner, L, Wang,
880 Y, Wilbur, WJ, Yaschenko, E, Ye, J. 2011. Database resources of the national center for
881 biotechnology information. Nucleic Acids Res 39:38.

882 67. Chen Y, Cao, X, Loh, KH, Slavoff, SA. 2023. Chemical labeling and proteomics for
883 characterization of unannotated small and alternative open reading frame-encoded
884 polypeptides. Biochem Soc Trans 51:1071–1082.

885 68. Will S, Joshi, T, Hofacker, IL, Stadler, PF, Backofen, R. 2012. LocARNA-P: Accurate boundary
886 prediction and improved detection of structural RNAs. RNA 18:900–914.

887 69. Wright PR, Georg, J, Mann, M, Sorescu, DA, Richter, AS, Lott, S, Kleinkauf, R, Hess, WR,
888 Backofen, R. 2014. CopraRNA and IntaRNA: Predicting small RNA targets, networks and
889 interaction domains. Nucleic Acids Res 42:119.

890 70. Allers T, Hien-Ping N, Mevarech M, Lloyd RG. 2004. Development of additional selectable
891 markers for the halophilic archaeon *Haloferax volcanii* based on the *leuB* and *trpA* genes. Appl
892 Environ Microbiol 70:943–953.

893 71. Rawls KS, Martin JH, Maupin-Furlow JA. 2011. Activity and transcriptional regulation of
894 bacterial protein-like glycerol-3-phosphate dehydrogenase of the haloarchaea in *Haloferax*
895 *volcanii.* J Bacteriol 193:4469–4476.

896 72. Wang X, Liu, Q, Zhang, B. 2014. Leveraging the complementary nature of RNA-seq and
897 shotgun proteomics data. Proteomics 14:2676–2687.

898 73. de Sousa Abreu R, Penalva, LO, Marcotte, EM, Vogel, C. 2009. Global signatures of protein
899 and mRNA expression levels. Mol Biosyst 5:1512–1526.

900 74. Zhong J, Xiao, C, Gu, W, Du, G, Sun, X, He, Q, Zhang, G. 2015. Transfer RNAs mediate the
901 rapid adaptation of *Escherichia coli* to oxidative stress. PLOS Genetics 11:e1005302.

902 75. Zhu M, Dai, X. 2019. Maintenance of translational elongation rate underlies the survival of
903 *Escherichia coli* during oxidative stress. Nucleic Acids Res 47:7592–7604.

904 76. Baliga NS, Bjork, SJ, Bonneau, R, Pan, M, Iloanusi, C, Kottemann, MCH, Hood, L, DiRuggiero,
905 J. 2004. Systems level insights into the stress response to UV radiation in the halophilic
906 archaeon *Halobacterium* NRC-1. Genome Res 14:1025–1035.

907 77. Warner JR. 1999. The economics of ribosome biosynthesis in yeast. Trends Biochem Sci
908 24:437–440.

909 78. Bąkowska-Żywicka K, Kasprzyk, M, Twardowski, T. 2016. tRNA-derived short RNAs bind to
910 *Saccharomyces cerevisiae* ribosomes in a stress-dependent manner and inhibit protein
911 synthesis in vitro. FEMS Yeast Res 16:fow077.

912 79. Holcik M, Sonenberg, N. 2005. Translational control in stress and apoptosis. Nat Rev Mol
913 Cell Biol 6:318–327.

914 80. Whitehead K, Kish, A, Pan, M, Kaur, A, Reiss, DJ, King, N, Hohmann, L, DiRuggiero, J, Baliga,
915 NS. 2006. An integrated systems approach for understanding cellular responses to gamma
916 radiation. Molecular Systems Biology 2:47.

917 81. Ghosal D, Omelchenko, MV, Gaidamakova, EK, Matrosova, VY, Vasilenko, A, Venkateswaran,
918 A, Zhai, M, Kostandarithes, HM, Brim, H, Makarova, KS. 2005. How radiation kills cells: Survival
919 of *Deinococcus radiodurans* and *Shewanella oneidensis* under oxidative stress. FEMS Microbiol
920 Rev 29:361–375.

921 82. Liu Y, Zhou, J, Omelchenko, MV, Beliaev, AS, Venkateswaran, A, Stair, J, Wu, L, Thompson,
922 DK, Xu, D, Rogozin, IB. 2003. Transcriptome dynamics of *Deinococcus radiodurans* recovering
923 from ionizing radiation. Proc Natl Acad Sci U S A 100:4191–4196.

924 83. Al-Fageeh MB, Smales, CM. 2009. Cold-inducible RNA binding protein (CIRP) expression is
925 modulated by alternative mRNAs. RNA 15:1164–1176.

926 84. Costa ED, Chai, Y, Winans, SC. 2012. The quorum-sensing protein TraR of *Agrobacterium*
927 *tumefaciens* is susceptible to intrinsic and TraM-mediated proteolytic instability. Mol Microbiol
928 84:807–815.

929 85. Dessaux Y, Faure, D. 2018. Quorum sensing and quorum quenching in *Agrobacterium*: A
930 "go/no go system"? Genes (Basel) 9:210.

931 86. Turnbough CLJ. 2019. Regulation of bacterial gene expression by transcription attenuation.
932 Microbiol Mol Biol Rev 83:e00019–19.

933 87. Xiu Z, Chang, Z, Zeng, A. 2002. Nonlinear dynamics of regulation of bacterial trp operon:
934 Model analysis of integrated effects of repression, feedback inhibition, and attenuation.
935 Biotechnol Prog 18:686–693.

936 88. Nagel C, Machulla, A, Zahn, S, Soppa, J. 2019. Several one-domain zinc finger μ-proteins of
937 *Haloferax volcanii* are important for stress adaptation, biofilm formation, and swarming. Genes
938 10:361.

939 89. Aoyama JJ, Raina, M, Zhong, A, Storz, G. 2022. Dual-function spot 42 RNA encodes a 15–
940 amino acid protein that regulates the CRP transcription factor. Proc Natl Acad Sci U S A
941 119:e2119866119.

942 90. Raina M, King, A, Bianco, C, Vanderpool, CK. 2018. Dual-function RNAs. Microbiol Spectr
943 6:10.1128/microbiolspec.rwr–2018.

944 91. Lloyd CR, Park, S, Fei, J, Vanderpool, CK. 2017. The small protein SgrT controls transport
945 activity of the glucose-specific phosphotransferase system. J Bacteriol 199:e00869–16.

946 92. Tufail MA, Jordan, B, Hadjeras, L, Gelhausen, R, Cassidy, L, Habenicht, T, Gutt, M, Hellwig, L,
947 Backofen, R, Tholey, A, Sharma, CM, Schmitz, RA. 2024. Uncovering the small proteome of
948 *Methanosarcina mazei* using ribo-seq and peptidomics under different nitrogen conditions. Nat
949 Commun 15:8659.

950 93. Raina M, Aoyama, JJ, Bhatt, S, Paul, BJ, Zhang, A, Updegrove, TB, Miranda-Ríos, J, Storz, G.
951 2022. Dual-function AzuCR RNA modulates carbon metabolism. Proc Natl Acad Sci U S A
952 119:e2117930119.

953 94. Guttman M, Russell, P, Ingolia, NT, Weissman, JS, Lander, ES. 2013. Ribosome profiling
954 provides evidence that large noncoding RNAs do not encode proteins. Cell 154:240–251.

955 95. Gelhausen R, Müller, T, Svensson, SL, Alkhnbashi, OS, Sharma, CM, Eggenhofer, F, Backofen,
956 R. 2022. RiboReport - benchmarking tools for ribosome profiling-based identification of open
957 reading frames in bacteria. Brief Bioinform 23:bbab549.

958 96. Gebetsberger J, Zywicki, M, Künzi, A, Polacek, N. 2012. tRNA-derived fragments target the
959 ribosome and function as regulatory non-coding RNA in *Haloferax volcanii*. Archaea
960 2012:260909.

961 97. Wyss L, Waser, M, Gebetsberger, J, Zywicki, M, Polacek, N. 2018. mRNA-specific translation
962 regulation by a ribosome-associated ncRNA in *Haloferax volcanii*. Sci Rep 8:12502.

963 98. Collins JA, Irnov, I, Baker, S, Winkler, WC. 2007. Mechanism of mRNA destabilization by the
964 *glmS* ribozyme. Genes Dev 21:3356–3368.

965 99. Desnoyers G, Morissette, A, Prévost, K, Massé, E. 2009. Small RNA-induced differential
966 degradation of the polycistronic mRNA iscRSUA. Embo J 28:1551–1561.

967 100. Märtens B, Manoharadas, S, Hasenöhrl, D, Manica, A, Bläsi, U. 2013. Antisense regulation
968 by transposon-derived RNAs in the hyperthermophilic archaeon *Sulfolobus solfataricus*. EMBO
969 Rep 14:527–533; 533.

970 101. Bernick DL, Dennis, PP, Höchsmann, M, Lowe, TM. 2012. Discovery of *Pyrobaculum* small
971 RNA families with atypical pseudouridine guide RNA features. RNA 18:402–411.

972 102. Goldberger O, Livny, J, Bhattacharyya, R, Amster-Choder, O. 2021. Wisdom of the crowds:
973 A suggested polygenic plan for small-RNA-mediated regulation in bacteria. iScience 24:103096.

974 103. Westermann AJ. 2018. Regulatory RNAs in virulence and host-microbe interactions.
975 Regulating with RNA in Bacteria and Archaea 6:305–337.

976 104. Gelsinger, DR, Dallon, E, DiRuggiero, J. 2022. Conversion of Ribosome-Protected mRNA to
977 DNA and Deep Sequencing for Ribosome Profiling in *Haloferax volcanii*, p. 223–242. *In* S.
978 Ferreira-Cerca (ed.), Archaea: Methods and Protocols. Springer US, New York, NY.
979 https://doi.org/10.1007/978-1-0716-2445-6_14.

980 105. Martin M. 2011. Cutadapt removes adapter sequences from high-throughput sequencing
981 reads. EMBnet.Journal 17:10-12.

982 106. Langmead B, Trapnell, C, Pop, M, Salzberg, SL. 2009. Ultrafast and memory-efficient
983 alignment of short DNA sequences to the human genome. Genome Biol 10:R25.

984 107. Li H, Handsaker, B, Wysoker, A, Fennell, T, Ruan, J, Homer, N, Marth, G, Abecasis, G,
985 Durbin, R, 1000 Genome Project Data Processing Subgroup. 2009. The sequence
986 alignment/map format and SAMtools. Bioinformatics 25:2078–2079.

987 108. Pertea M, Pertea, GM, Antonescu, CM, Chang, T, Mendell, JT, Salzberg, SL. 2015. StringTie
988 enables improved reconstruction of a transcriptome from RNA-seq reads. Nat Biotechnol
989 33:290–295.

990 109. Liao Y, Smyth, GK, Shi, W. 2014. featureCounts: An efficient general purpose program for
991 assigning sequence reads to genomic features. Bioinformatics 30:923–930.

992 110. Love MI, Huber, W, Anders, S. 2014. Moderated estimation of fold change and dispersion
993 for RNA-seq data with DESeq2. Genome Biol 15:550.

994 111. Babski J, Haas, KA, Näther-Schindler, D, Pfeiffer, F, Förstner, KU, Hammelmann, M, Hilker,
995 R, Becker, A, Sharma, CM, Marchfelder, A, Soppa, Jö. 2016. Genome-wide identification of
996 transcriptional start sites in the haloarchaeon *Haloferax volcanii* based on differential RNA-seq
997 (dRNA-seq). BMC Genomics 17:629.

998 112. Thomas PD, Ebert, D, Muruganujan, A, Mushayahama, T, Albou, L, Mi, H. 2022. PANTHER:
999 Making genome-scale phylogenetics accessible to all. Protein Sci 31:8–22.

1000 113. Moran HM, Manriquez-Sandoval, E, Sharma, P, Fried, SD, Gillilan, RE. 2024. Proteome-wide
1001 assessment of protein structural perturbations under high pressure. PRX Life 2:033011.

1002 114. To P, Whitehead, B, Tarbox, HE, Fried, SD. 2021. Nonrefoldability is pervasive across the E.
1003 coli proteome. J Am Chem Soc 143:11435–11448.

1004 115. Dyall-Smith, M. 2009. The Halohandbook – Protocols for haloarchaeal genetics. Available
1005 at https://haloarchaea.com/wp-content/uploads/2025/02/Halohandbook_2009_REV_v2.pdf.

1006 116. Fu X, Adams, Z, Maupin-Furlow, J. 2019. Assays for ubiquitin-like protein ligation and
1007 proteasome function in archaea. Methods Enzymol 619:161–178.

1008 117. Altschul SF, Gish, W, Miller, W, Myers, EW, Lipman, DJ. 1990. Basic local alignment search
1009 tool. J Mol Biol 215:403–410.

1010 118. Mann M, Wright, PR, Backofen, R. 2017. IntaRNA 2.0: Enhanced and customizable
1011 prediction of RNA–RNA interactions. Nucleic Acids Res 45:W435–W439.

1012 119. Livak KJ, Schmittgen, TD. 2001. Analysis of relative gene expression data using real-time
1013 quantitative PCR and the 2(-delta delta C(T)) method. Methods 25:402–408.

120. Perez-Riverol Y, Bandla, C, Kundu, DJ, Kamatchinathan, S, Bai, J, Hewapathirana, S, John, NS, Prakash, A, Walzer, M, Wang, S, Vizcaíno, JA. 2024. The PRIDE database at 20 years: 2025 update. Nucleic Acids Res 53:D543–D553.

Tables

Table 1. Annotated and novel small proteins encoded by sRNAs and detected by MS.

	Gene name	Genome location	Size (aa)	Start codon	Stop codon	RNA-seq TPMs		Ribo-seq TPMs	
						Control	Stress	Control	Stress
novel	**sRNA_7**	pHV3	31	CTG	TAG*	4.44	6.42	2.04	2.94
	sRNA_23	pHV4	70	CTG	TGA	11.55	17.46	5.86	12.98
	sRNA_80	chr	40	ATG	TAG	45.64	26.89	36.47	38.61
annotated	**sRNA_JD**	chr	56	ATG	TAA	203.29	307.16	163.10	497.56
	sRNA_KL	chr	57	ATG	TAA*	131.68	138.46	1207.81	405.01
	sRNA_81	chr	58	CTG	TAA	35.83	20.57	30.80	25.79
	sRNA_93	pHV1	116	ATG	TAG	262.20	276.16	627.41	421.53

Asterisks indicate sRNAs with stop codons outside of the annotated gene region.

Table 2. sRNAs tagged for Western blotting.

	Gene name	Genome location	sRNA length (nt)	smORF size (aa)	Stop codon	RNA-seq TPMs		Ribo-seq TPMs	
						Control	Stress	Control	Stress
MS-detected	**sRNA_KL**	chr	175	57	yes	131.68	138.46	1207.81	405.01
	sRNA_93	pHV1	507	116	yes	262.20	276.16	627.41	421.53
Putative smORFs	**sRNA_38**	pHV4	56	16	yes	18.19	40.62	40.61	120.04
	sRNA_83	chr	182	55	yes	288.90	270.63	22.64	81.98
	sRNA_20_ORF2	pHV4	189	21	yes	40.77	89.47	68.98	542.12
	sRNA_20_ORF4	pHV4	189	34	yes	40.77	89.47	68.98	542.12
High ribosome occupancy	**sRNA_61**	chr	111	32	no	4565.10	2281.40	1850.99	3381.31
	SHOxi	pHV3	254	73	no	346.33	1767.52	219.35	2034.76

sRNAs with “no” in the stop codon column had no stop codon contained in the predicted sRNA region as determined by ORFfinder.

1037 **Table 3.** sRNAs with differential ribosome occupancy or translational efficiency during oxidative
1038 stress.

	RNA-seq		Ribo-seq		TE		TPMs				footprint distributions		protein detection		
Name	fold change	p-value	fold change	p-value	fold change	p-value	RNA-seq control	RNA-seq stress	Ribo-seq control	Ribo-seq stress	coding cluster control	coding cluster stress	annotated protein	ArcPP detection	MS detected
sRNA_20	1.21	0.00	2.63	0.00	1.41	0.04	40.22	88.01	68.74	537.73	yes	yes	yes	no	no
sRNA_34	-0.44	0.22	-1.12	0.00	-0.70	0.26	19.44	15.34	12.93	7.52	yes	no	no	NA	no
sRNA_41	-0.93	0.00	-1.18	0.00	-0.27	0.66	46.64	24.21	11.62	6.65	no	no	yes	yes	no
sRNA_49	2.23	0.00	1.74	0.00	-0.50	0.57	37.41	195.67	127.06	525.30	no	no	no	NA	no
sRNA_58	0.40	0.37	1.23	0.01	0.81	0.39	21.45	34.76	41.31	135.96	no	no	no	NA	no
sRNA_60	-0.12	0.94	1.72	0.00	1.82	0.28	2491.07	1996.40	382.05	568.67	NA	no	no	NA	no
sRNA_61	-0.90	0.04	0.59	0.10	1.48	0.04	4496.30	2243.82	1843.17	3350.74	yes	yes	no	NA	no
sRNA_62	2.24	0.00	3.15	0.00	0.89	0.42	17.24	79.53	4.06	45.72	no	yes	no	NA	no
sRNA_71	-0.31	0.38	1.35	0.05	1.63	0.04	76.87	105.29	8.57	27.23	NA	NA	no	NA	no
sRNA_77	0.90	0.04	2.57	0.00	1.66	0.10	23.84	43.05	3.76	13.07	NA	no	no	NA	no
sRNA_83	0.06	0.89	1.59	0.00	1.52	0.03	284.91	266.25	22.57	81.26	no	no	no	NA	no
sRNA_95	1.14	0.00	1.61	0.00	0.46	0.56	21.16	45.04	9.43	33.82	no	no	no	NA	no
sRNA_96	1.65	0.00	1.59	0.00	-0.08	0.92	51.26	140.20	5.59	19.10	yes	yes	no	NA	no
sRNA_CD	0.95	0.01	1.50	0.00	0.53	0.44	83.53	141.43	168.64	569.29	no	yes	yes	yes	no
sRNA_JD	0.68	0.20	1.33	0.01	0.64	0.57	200.14	301.88	162.34	493.83	yes	yes	yes	yes	yes
sRNA_KL	0.16	0.57	-1.93	0.00	-2.12	0.00	129.94	136.19	1203.27	401.61	yes	yes	yes	yes	yes
sRNA_SHOxi	2.46	0.00	2.89	0.00	0.42	0.72	341.52	1738.88	218.70	2017.74	yes	no	no	NA	no

1039
1040 Fold change refers to $\log_2$ fold change, and p-value refers to the adjusted p-value.
1041
1042 **Table 4.** Putative mRNA targets with differential ribosome occupancy or TE during oxidative stress.

			RNA-seq		Ribo-seq		TE		TPMs			
	Target Name	Function	Fold Change	p-value	Fold Change	p-value	Fold Change	p-value	RNA-seq Control	RNA-seq Stress	Ribo-seq Control	Ribo-seq Stress
sRNA_58	HVO_RS04540	hypothetical protein	-1.21	0.00	-1.21	0.00	-0.02	0.98	326.20	169.80	370.97	208.87
	HVO_RS13165	ABC transporter permease	-1.64	0.00	-1.27	0.00	0.36	0.51	640.15	188.77	85.81	45.53
	HVO_RS17485	D-2-hydroxyacid dehydrogenase	-1.01	0.00	-1.60	0.00	-0.61	0.07	27.50	47.10	58.33	27.88
	HVO_RS17805	hypothetical protein	1.00	0.00	1.46	0.00	0.45	0.45	54.93	91.69	36.61	98.47
	HVO_RS19470	hypothetical protein	1.33	0.01	-0.65	0.05	-2.01	0.01	7.57	15.74	55.04	44.71
sRNA_77	HVO_RS05320	YccF domain-containing protein	1.01	0.00	1.37	0.00	0.34	0.62	26.87	53.00	37.93	121.84
	HVO_RS06805	co-chaperone YbbN	0.62	0.06	-0.66	0.03	-1.30	0.01	1088.48	1614.45	2937.95	2326.41
	HVO_RS07705	hypothetical protein	-0.52	0.09	0.80	0.07	1.31	0.04	51.84	33.24	11.22	23.01
	HVO_RS08415	amidohydrolase family protein	-0.88	0.00	-1.87	0.00	-1.01	0.03	82.41	82.17	87.53	55.80
	HVO_RS09105	2Fe-2S domain-containing protein	-0.24	0.31	-1.24	0.00	-1.01	0.05	67.63	53.64	76.35	40.75
	HVO_RS11380	hypothetical protein	1.06	0.00	2.71	0.00	1.63	0.04	21.14	49.53	68.11	579.99
	HVO_RS11455	BMP family protein	-0.72	0.00	-1.78	0.00	-1.08	0.05	1322.62	720.75	1618.05	586.70
	HVO_RS13145	hypothetical protein	0.93	0.00	1.06	0.00	0.11	0.86	193.21	286.04	47.28	123.46
	HVO_RS14580	dehydrorhamnose epimerase family protein	-0.76	0.03	-1.88	0.00	-1.14	0.07	1726.87	885.36	986.87	329.83
	HVO_RS15315	hypothetical protein	-0.73	0.00	0.74	0.03	1.46	0.00	133.96	75.10	13.40	25.06
	HVO_RS17930	30S ribosomal protein S28e	-1.01	0.00	-1.63	0.00	-0.63	0.13	8234.66	3814.46	1902.49	770.44
	HVO_RS18350	hypothetical protein	1.10	0.00	1.19	0.02	0.07	0.94	19.56	38.77	6.65	17.79
	HVO_RS18595	GNAT family N-acetyltransferase	0.27	0.39	1.05	0.00	0.76	0.12	30.92	27.85	9.31	23.79
	HVO_RS18740	hypothetical protein	0.16	0.66	1.18	0.00	0.99	0.08	68.49	68.32	17.95	42.57
	HVO_RS20570	rubrerythrin-like domain-containing protein	0.97	0.00	3.78	0.00	2.79	0.00	50.42	49.15	17.52	161.98
sRNA_83	HVO_RS00230	methyltransferase	-1.08	0.00	-1.08	0.00	-0.01	0.98	219.52	94.40	163.37	97.06
	HVO_RS00700	ABC transporter substrate-binding protein	-2.13	0.00	-2.70	0.00	-0.59	0.42	190.15	38.32	819.59	157.72
	HVO_RS01670	racemase enzyme family protein	1.66	0.00	1.20	0.01	-0.47	0.60	4.57	12.69	6.18	18.40
	HVO_RS03935	ring-cleaving dioxygenase	0.98	0.00	1.44	0.00	0.44	0.36	36.14	63.65	24.10	83.36
	HVO_RS04155	hypothetical protein	0.96	0.08	2.51	0.00	1.55	0.09	36.47	27.77	18.03	36.31
	HVO_RS04735	hypothetical protein	-0.12	0.72	1.10	0.00	1.21	0.01	50.36	45.95	18.86	51.67
	HVO_RS05345	thermosome subunit alpha	-1.06	0.00	-1.58	0.00	-0.53	0.37	4645.21	2047.07	6582.65	2681.76
	HVO_RS08545	SPFH domain-containing protein	0.46	0.04	1.25	0.00	0.77	0.10	295.03	436.26	65.36	202.53
	HVO_RS08645	NAD(P)-dependent dehydrogenase	-0.74	0.00	-1.63	0.00	-0.91	0.01	143.06	78.46	197.19	80.87
	HVO_RS13905	serine--tRNA ligase	-0.51	0.02	-1.27	0.00	-0.77	0.07	384.53	246.71	547.21	295.37
	HVO_RS13930	SIMPL domain-containing protein	0.99	0.00	1.69	0.00	0.68	0.17	65.12	120.33	24.14	91.85
	HVO_RS17570	HpcH/HpaI aldolase/citrate lyase family protein	0.96	0.01	1.87	0.00	0.89	0.38	133.65	232.04	49.88	213.11
	HVO_RS19230	ABC transporter ATP-binding protein	-1.35	0.00	-1.65	0.00	-0.32	0.55	38.24	18.34	66.16	27.28

1043
1044 Fold change refers to $\log_2$ fold change, and p-value refers to the adjusted p-value.

Figures

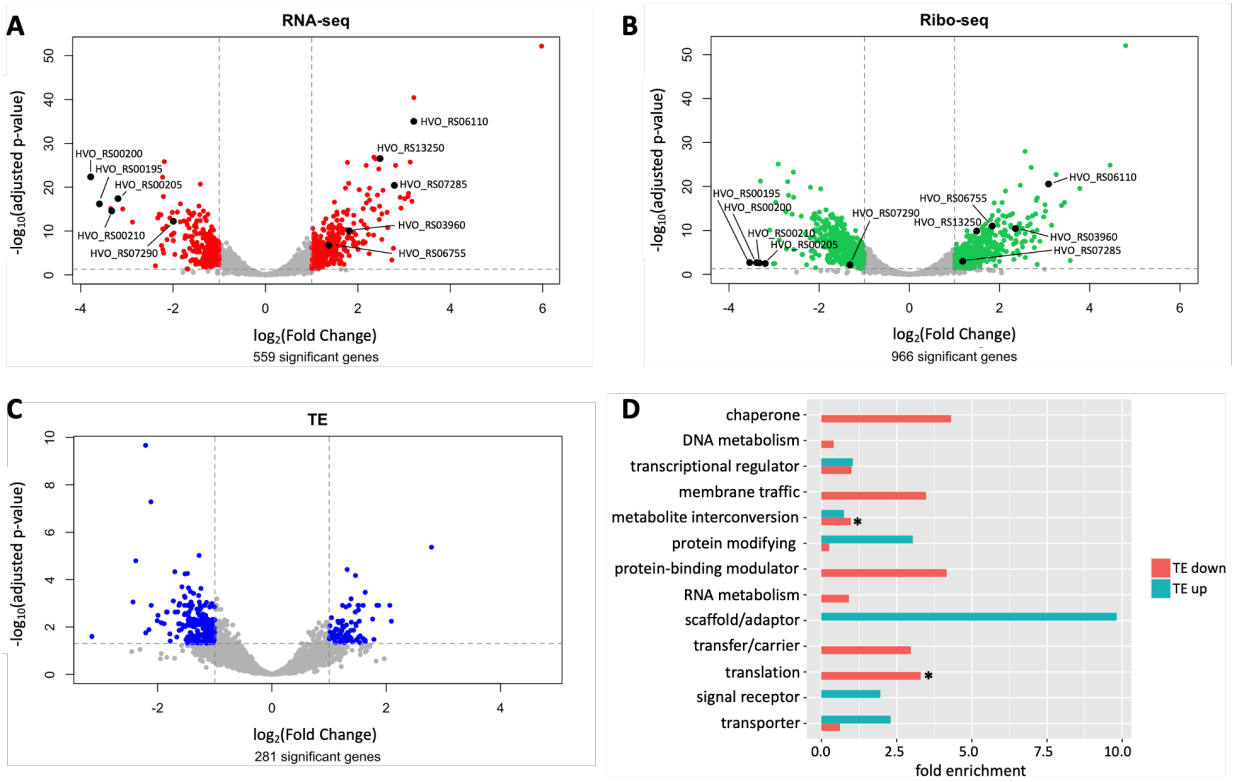

Figure 1. Comparison of genes with differential transcription, ribosome occupancy, and translation during oxidative stress. Volcano plots of $\log_2$ fold changes and corresponding $-\log_{10}$ p-values of transcript abundances (A), ribosome occupancies (B), and translation efficiency (C) comparing stress vs no stress conditions. Red, green, and blue colored points highlight transcripts with differential expression (adjusted p-value <0.05 and absolute $\log_2$ fold change >1). Fold change and p-values were calculated using DESeq2. Labeled black points indicate genes previously shown to be involved in oxidative stress response. All other genes are shown in gray. D. Functional categories (protein class) of genes with differential TE during oxidative stress. Functions of significant genes were categorized using PANTHER generic mapping based on homology. Enrichment of functional categories in upregulated (TE up) or downregulated (TE down) genes compared to all annotated genes was calculated using the total number of PANTHER hits for each group (2061 for all annotated genes, 99 for TE down, and 42 for TE up). Asterisks indicate significant categories (translation) or categories that contain significantly enriched subcategories (ribosomal proteins; peroxidases).

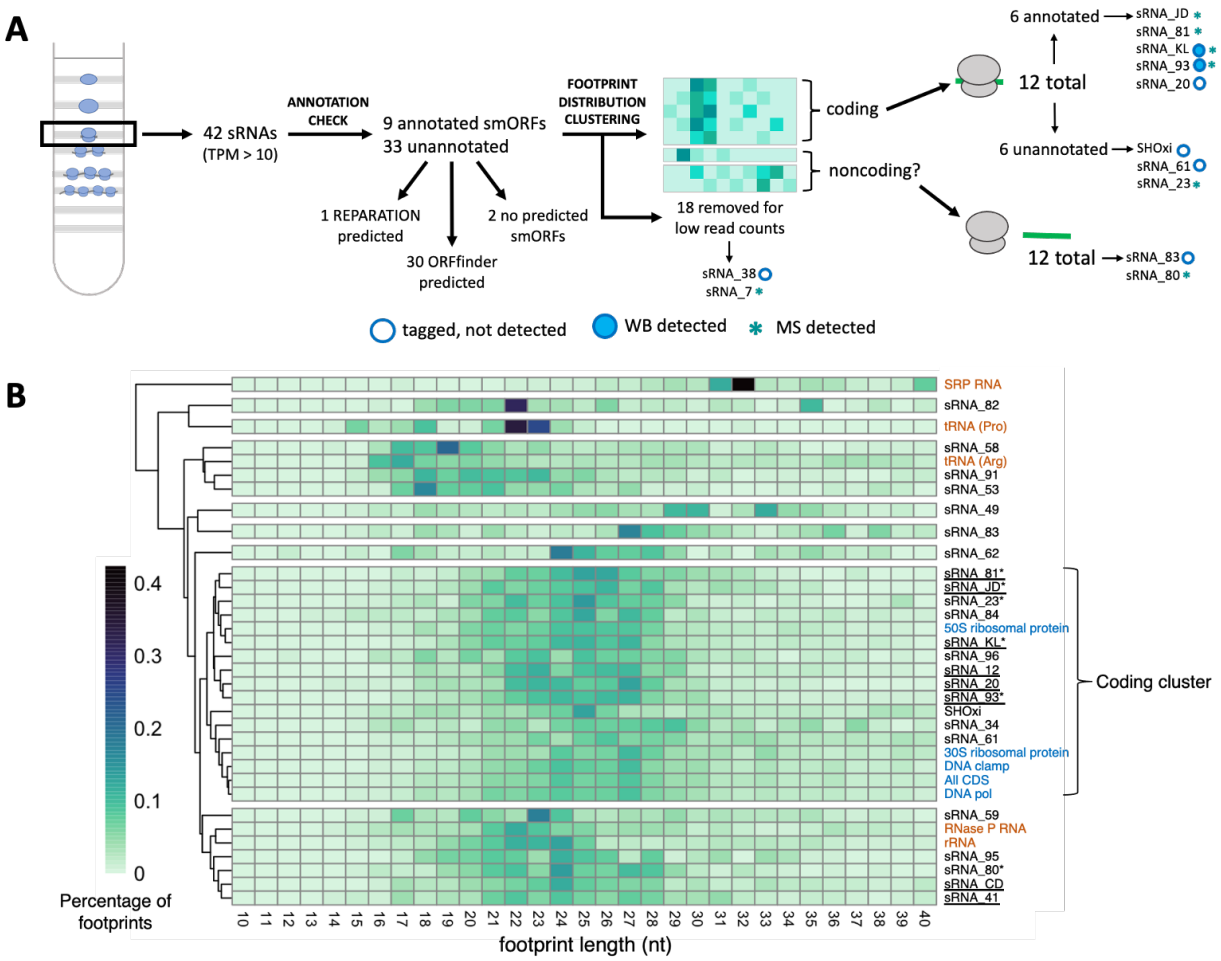

Figure 2. Ribosome footprint length distributions and sRNAs with ribosome occupancy. A. Schematic of analyses to assess the coding potential for sRNAs with ribosome occupancy, starting with the isolation of monosome fractions during ribosome profiling. B. Clustered heatmap of ribosome footprint length distributions for sRNAs, coding genes, and noncoding genes with ribosome occupancy under control conditions. Darker colors indicate higher read percentage. Known coding genes are shown in blue, known noncoding genes in orange, and sRNAs in black. sRNAs with annotated proteins are underlined. sRNAs for which peptides have been detected by MS are marked with an asterisk. Percentages for 'All CDS' were calculated using sum read counts of all coding genes.

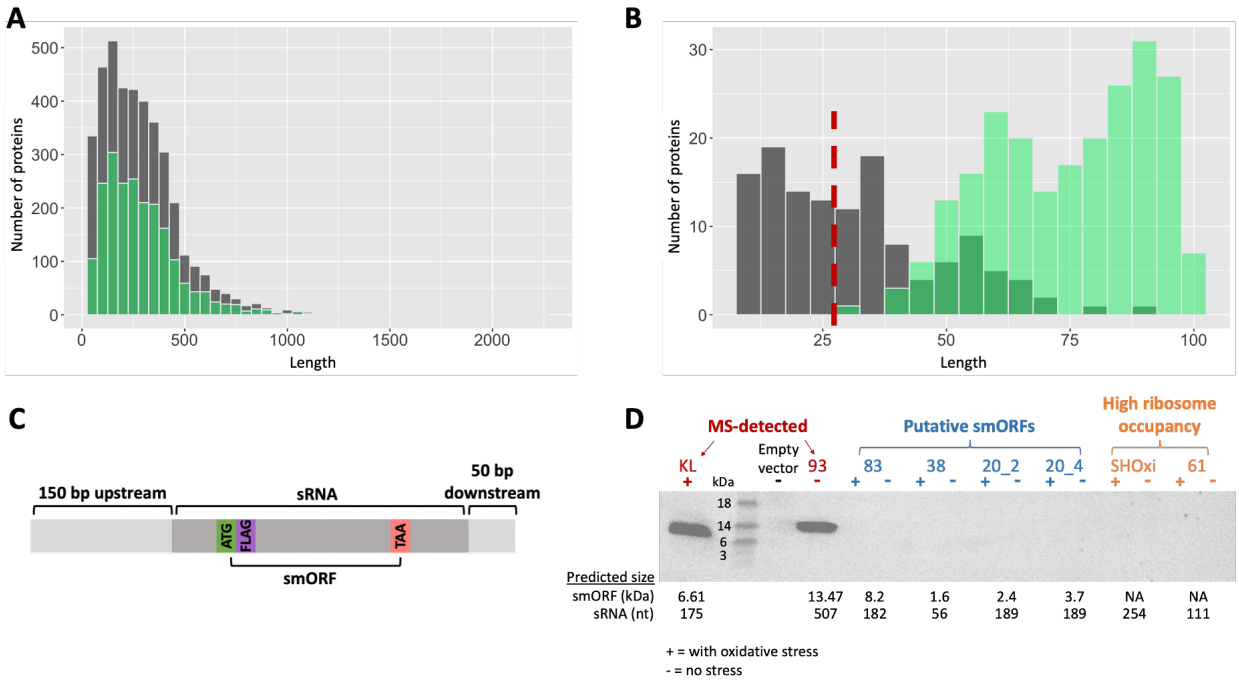

Figure 3. Discovery of novel small proteins encoded in sRNAs. A. Overlapping histogram of protein length (aa) for the *H. volcanii* annotated proteome (gray) and proteins detected by MS (overlaid in green). B. Overlapping histogram of protein length (aa) for putative peptides (predicted using NCBI ORF finder) encoded by sRNAs (gray) and small proteins detected by MS (overlaid in green). Detection cutoff of 30aa is indicated by red dashed line. C. Cloning strategy for tagging sRNAs for Western blot analysis. FLAG indicates the location of the 3xFLAG-tag. D. Western blot of tagged sRNAs. + indicates samples treated with hydrogen peroxide and - indicates control samples.

1081

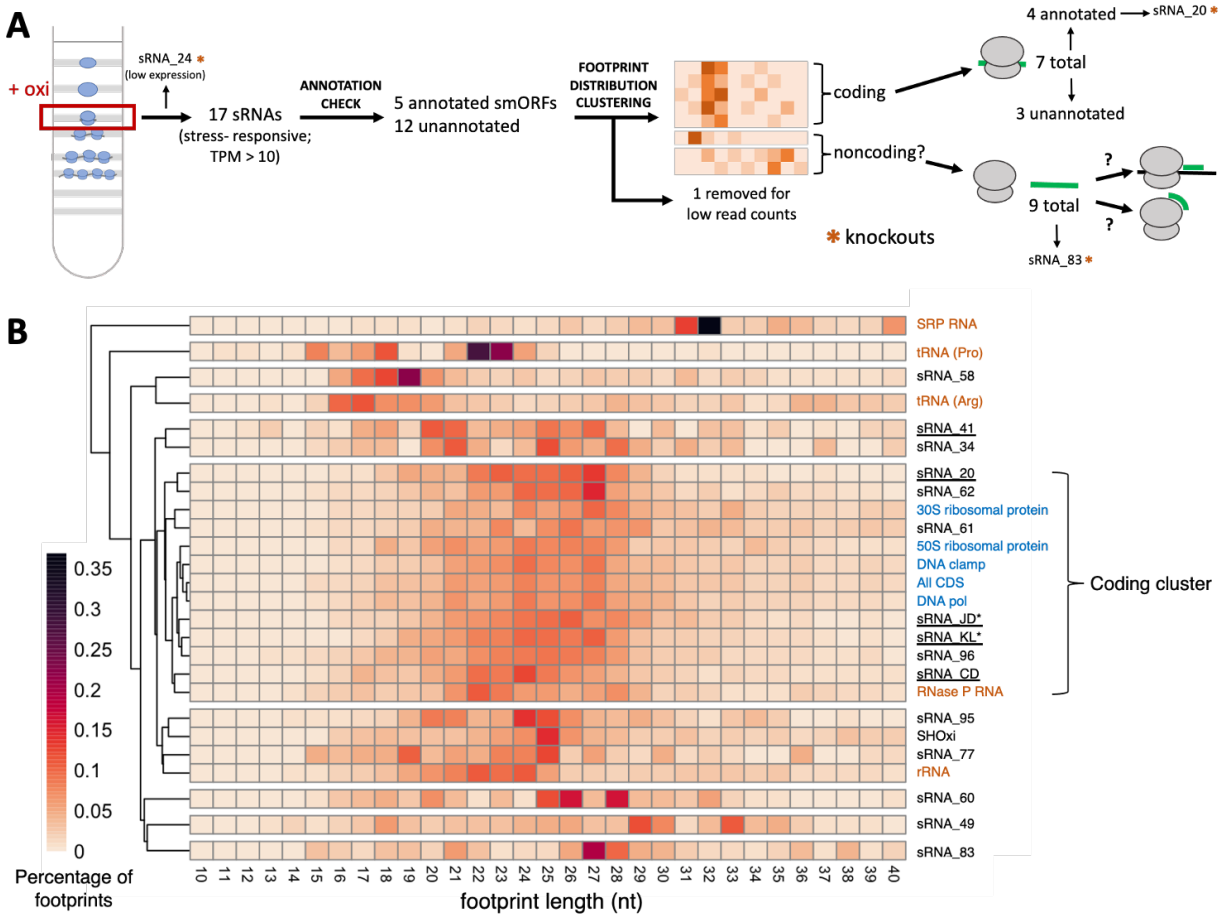

1082

1083 **Figure 4. Ribosome footprint length distributions and stress-responsive sRNAs with ribosome**
1084 **occupancy.** A. Schematic of analyses to assess the coding potential for sRNAs with ribosome
1085 occupancy, starting with the isolation of monosome fractions on a sucrose gradient using
1086 samples treated with oxidative stress. B. Clustered heatmaps of ribosome footprint length
1087 distributions for sRNAs, coding genes, and noncoding genes with ribosome occupancy under
1088 oxidative stress. Darker colors indicate higher read percentage. Known coding genes are shown
1089 in blue, known noncoding genes in orange, and sRNAs in black. sRNAs with annotated proteins
1090 are underlined. sRNAs for which peptides have been detected by MS are marked with an
1091 asterisk. Percentages for 'All CDS' were calculated using sum read counts of all coding genes.

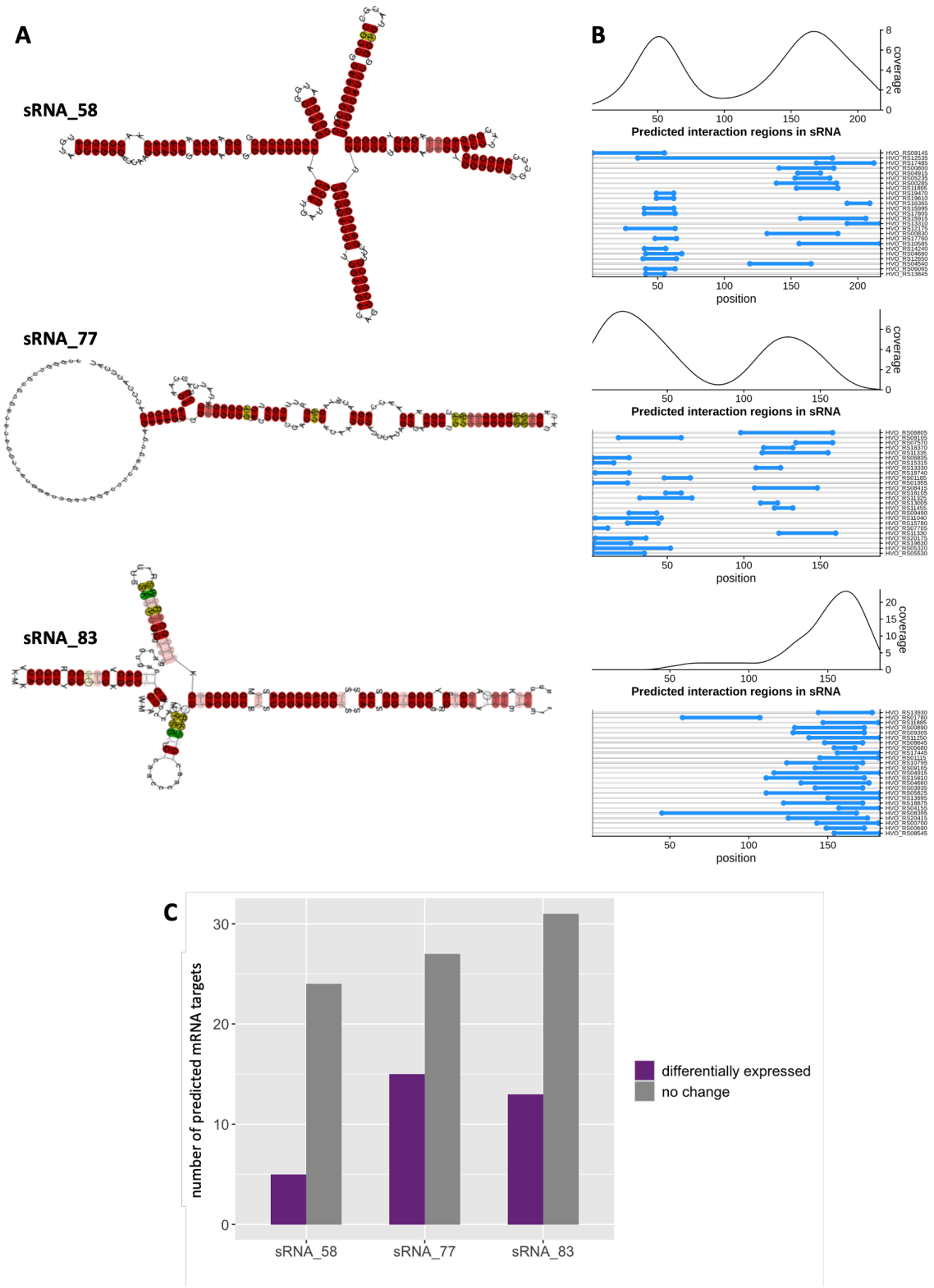

1092

1093 **Figure 5. Characterization of stress-responsive sRNAs with ribosome occupancy.** A. Consensus
1094 RNA structural predictions for sRNAs with no evidence of coding potential were generated
1095 using LocARNA. Colored bases indicate sequence and structural conservation of compatible

1096 base pairs within the predicted structure (see Fig. S7). Colors correspond to number (red: 1,
1097 yellow: 2, green: 3) of base pair types (C-G, G-C, A-U, U-A, G-U, or U-G) with red being the most
1098 highly conserved and green the least conserved. Color saturation decreases with the number of
1099 incompatible base pairs. B. IntaRNA was used to predict putative mRNA targets (Tables S14-16).
1100 Blue lines indicate putative binding regions along the sRNA. Curves depict coverage of putative
1101 binding regions along the sRNA. C. Bar chart of predicted mRNA targets ($p < 0.01$) with
1102 differential ribosome occupancy or TE during oxidative stress (purple). The number of predicted
1103 targets that are unaffected by oxidative stress are shown in gray.
1104